

Titre: Semi-Analytical Method for g-Function Calculation of bore fields with series- and parallel-connected boreholes
Title:

Auteurs: Massimo Cimmino
Authors:

Date: 2019

Type: Article de revue / Article

Référence: Cimmino, M. (2019). Semi-Analytical Method for g-Function Calculation of bore fields with series- and parallel-connected boreholes. Science and Technology for the Built Environment, 25(9), 1007-1022.
Citation: <https://doi.org/10.1080/23744731.2019.1622937>

Document en libre accès dans PolyPublie

Open Access document in PolyPublie

URL de PolyPublie: <https://publications.polymtl.ca/5503/>
PolyPublie URL:

Version: Version finale avant publication / Accepted version
Révisé par les pairs / Refereed

Conditions d'utilisation: Tous droits réservés / All rights reserved
Terms of Use:

Document publié chez l'éditeur officiel

Document issued by the official publisher

Titre de la revue: Science and Technology for the Built Environment (vol. 25, no. 9)
Journal Title:

Maison d'édition: Taylor & Francis
Publisher:

URL officiel: <https://doi.org/10.1080/23744731.2019.1622937>
Official URL:

Mention légale: This is an Accepted Manuscript of an article published by Taylor & Francis in Science and Technology for the Built Environment (vol. 25, no. 9) in 2019, available online:
Legal notice: <https://doi.org/10.1080/23744731.2019.1622937>

***g*-Functions of bore fields with series- and parallel-connected boreholes**

MASSIMO CIMMINO^{1*}

¹*Department of Mechanical Engineering, Polytechnique Montréal, Montréal, QC, Canada*

*A semi-analytical method for the calculation of *g*-functions of bore fields with mixed arrangements of series- and parallel-connected boreholes is presented. Borehole wall temperature variations are obtained from the temporal and spatial superposition of the finite line source (FLS) solution. The FLS solution is coupled to a quasi-steady-state solution of the fluid temperature profiles in the boreholes, considering the piping connections between the boreholes. The dimensionless borehole wall temperatures in the bore field and the inlet fluid temperature are obtained from the simultaneous solution of the heat transfer inside and outside the boreholes. The effective borehole wall temperature, i.e. the *g*-function, is defined based on the dimensionless inlet fluid temperature and a newly introduced effective bore field thermal resistance. The *g*-function evaluation method is validated against the DST model and its use is demonstrated in a sample simulation of a seasonal thermal energy storage system.*

Introduction

The design of geothermal bore fields is facilitated by the accurate prediction of fluid and ground temperatures during their operation. The simulation of geothermal bore fields can be achieved by temporally superimposing thermal response factors, or *g*-functions, to obtain the fluid and ground temperature variations over the design period, e.g. 20 years or more. *g*-Functions are also employed in direct design methods, such as the ASHRAE method (ASHRAE 2015).

By definition, *g*-functions are step-response functions that give the relation between the heat extraction rate in the bore field and the effective temperature variation at the borehole walls. The *g*-function of a particular bore field may then be superimposed in time to obtain the effective borehole wall temperature variation due to a variable heat extraction rate in the bore field:

$$T_b^*(t) = T_0 - \frac{1}{2\pi k_s} \int_0^t \bar{Q}'(t - t') \frac{dg}{dt}(t') dt' \quad (1)$$

Massimo Cimmino is an assistant professor.

*Corresponding author e-mail: massimo.cimmino@polymtl.ca

where T_b^* is the effective borehole wall temperature, T_0 is the undisturbed ground temperature, \bar{Q}' is the average heat extraction rate per unit borehole length and g is the g -function of the bore field. The effective borehole wall temperature is related to the mean fluid temperature in the bore field through the bore field thermal resistance:

$$\bar{T}_f(t) = T_b^*(t) - R_{field}^* \bar{Q}'(t) \quad (2)$$

where $\bar{T}_f = 0.5(T_{f,in} + T_{f,out})$ is the arithmetic mean of the inlet and outlet fluid temperature in the bore field and R_{field}^* is the effective bore field thermal resistance.

In fields of boreholes of equal dimensions (length and radius) with the same U-tube pipe configurations, connected in parallel and receiving evenly distributed fluid mass flow rates, the effective borehole wall temperature is typically equal to the overall average borehole wall temperature and the effective bore field thermal resistance is equal to the effective borehole thermal resistance R_b^* (equal for all boreholes). Bore fields with series connections between boreholes may feature important differences in temperature at the borehole walls and the overall average borehole wall temperature is then not representative of heat transfer between the fluid and the ground. The effective bore field thermal resistance also needs to be adjusted to account for the variation of fluid temperatures in series-connected boreholes.

The concept of g -functions was introduced by Eskilson (1987). The original g -functions were obtained numerically using a finite difference method by simulating the temperature variations at the borehole walls caused by a constant total heat extraction rate from the bore field. A condition of uniform temperature at the borehole walls, equal for all boreholes, was imposed. This condition stems from the assumptions that (i) the borehole thermal resistance is sufficiently small that the borehole wall temperature is close to the fluid temperature, and (ii) that the fluid mass flow rate is sufficiently large that the fluid temperature variations inside the boreholes are small. From these assumptions, for bore fields of parallel-connected boreholes, the borehole wall temperature is close to uniform and equal for all boreholes. For large bore fields with large amounts of boreholes, the generation of g -functions becomes computationally intensive.

Since then, analytical methods have been employed to approximate g -functions. Eskilson (1987) proposed using the finite line source (FLS) solution to approximate the thermal response of a single borehole. Zeng et al. (2002) later proposed the spatial superposition of the FLS to obtain g -functions of bore fields with

multiple boreholes. Lamarche and Beauchamp (2007a) and Claesson and Javed (2011) developed simplified formulations of the FLS solution to compute the average (over the length) borehole wall temperature. The limitation of the FLS solution is that it considers uniform heat extraction rate along the boreholes, which does not correspond to the uniform borehole wall temperature condition of Eskilson (1987) and leads to an overestimation of the g -function (Fossa 2011). The variation of heat extraction rates along the boreholes can be represented by vertically dividing the borehole into segments and modelling each of the segments with the FLS solution (Cimmino and Bernier 2014; Cimmino, Bernier, and Adams 2013; Lamarche 2017b; Cimmino 2018c), thereby respecting the condition of uniform borehole wall temperature in the calculation of g -functions. The calculation of g -functions can be accelerated by the joint use of Chebyshev polynomials or by the simultaneous evaluation of the g -functions at all times using a block matrix formulation (Dusseault, Pasquier, and Marcotte 2018). g -Functions were also evaluated numerically using the finite element method by Monzó et al. (2015) and by Naldi and Zanchini (2019). The validity of the condition of uniform borehole wall temperature was investigated by Cimmino (2015) using an FLS-based method and by Monzó et al. (2018) using a finite element method. It was found that, as the borehole thermal resistance is reduced, the borehole wall temperatures tend to uniformity.

Analytical and semi-analytical extensions of the g -functions have been proposed to extend their validity outside of pure conduction in uniform isotropic ground, and to consider short-term dynamics of the boreholes. Short-term one-dimensional radial analytical solutions that model the fluid flowing inside U-tubes as a single equivalent diameter pipe have been proposed in the works of Beier and Smith (2003), Lamarche and Beauchamp (2007b), Bandyopadhyay et al. (2008), Javed and Claesson (2011), Lamarche (2015). Line sources in composite media have been proposed by Li and Lai (2013; 2012a) to model the effect of the thermal properties of the grout material. A moving finite line source to model boreholes under the influence of groundwater flow was proposed by Molina-Giraldo et al. (2011). A finite line source solution applicable to anisotropic ground was proposed by Li and Lai (2012b). Layered subsurface properties were considered in the works of Abdelaziz et al. (2014), Hu (2017) and Erol and François (2018). Finite line source solutions for inclined boreholes were proposed in the works of Cui et al. (2006), Marcotte and Pasquier (2009) and Lamarche (2011), and were used by Lazzarotto (2016) to obtain g -functions with uniform borehole wall temperature.

The aforementioned models are only applicable to parallel-connected boreholes. Series connections between boreholes are common in borehole thermal energy storage (BTES) systems, where a temperature gradient is established in the ground for efficient charging and discharging of the storage, typically in a cylindrical volume. The most commonly used model for the simulation of BTES is the duct ground heat storage (DST) model (Pahud and Hellström 1996), which assumes that the boreholes are uniformly distributed in a cylindrical volume. The storage and fluid temperatures are obtained by the numerical solution of local and global problems. A limitation of the DST model is that the position and piping arrangement of the boreholes cannot be prescribed. A finite line source method to evaluate g -functions of fields of borehole with a mix of series and parallel connections was proposed by Marcotte and Pasquier (2014). However, their method does not consider the axial variations of heat transfer rates along the boreholes and may thus overestimate the long-term variations of borehole wall temperatures.

The objective of this paper is to obtain g -functions for fields of boreholes with a mixed arrangement of series and parallel connections between the boreholes. The heat transfer process in the bore field is divided into two regions: (1) unsteady heat conduction between the borehole wall and the surrounding ground, and (2) quasi-steady-state heat transfer between the heat carrier fluid and the borehole walls. The two regions are joined by a condition of continuity of temperature and heat transfer rate at the borehole walls. The paper expands on earlier work (Cimmino 2018b), and includes expressions to evaluate fluid temperatures and heat extraction rates in boreholes with axially varying borehole wall temperature as well as a sample simulation of a borehole thermal energy storage consisting of 144 boreholes.

The proposed method provides a contribution to the works of Marcotte and Pasquier (2014) who obtained thermal response factors of fields of series- and parallel-connected boreholes, and to the works of Cimmino (2015) and Monzó (2018) who showed the effect of the borehole thermal resistance on the long-term temperature changes in geothermal bore fields. An extension of the method of Cimmino (2016) is presented, providing simplified expressions to obtain fluid temperature and heat extraction rate profiles along geothermal boreholes. The simplified expressions, applied to series- and parallel-connected boreholes, provide a contribution to the network-based simulation methods of Lazzarotto (2014), Lamarche (2017a) and Cimmino (2018a) by reducing the size of the system of equations to be solved for the fluid and borehole wall temperatures.

Methodology

A field of $N_b = 3$ vertical boreholes is shown on Figure 1. Each borehole i has a length L_i , is buried at a distance D_i from the ground surface, and is located at coordinates (x_i, y_i) . All boreholes have the same radius r_b . Heat carrier fluid enters the bore field at a temperature $T_{f,in}$ and leaves the bore field at a temperature $T_{f,out}$ with a total mass flow rate \dot{m} . The ground has a thermal conductivity k_s , a thermal diffusivity α_s and is initially at an undisturbed temperature T_0 . In the context of this paper, boreholes may be connected in a mixed arrangement of parallel and series connections between the boreholes. Each borehole may have one or multiple U-tube pipes connected in series or in parallel. In Figure 1, boreholes 1 and 3 each receive the fluid at a temperature $T_{f,in,1} = T_{f,in,3} = T_{f,in}$ corresponding to the inlet field temperature and at mass flow rates \dot{m}_1 and \dot{m}_3 (with $\dot{m}_1 + \dot{m}_3 = \dot{m}$), respectively. Borehole 2 receives the fluid at a temperature $T_{f,in,2} = T_{f,out,1}$ corresponding to the outlet of borehole 1 and at a mass flow rate $\dot{m}_2 = \dot{m}_1$. The outlet field temperature $T_{f,out} = (\dot{m}_2 T_{f,out,2} + \dot{m}_3 T_{f,out,3}) / \dot{m}$ is the result of mixing of the fluid leaving boreholes 2 and 3.

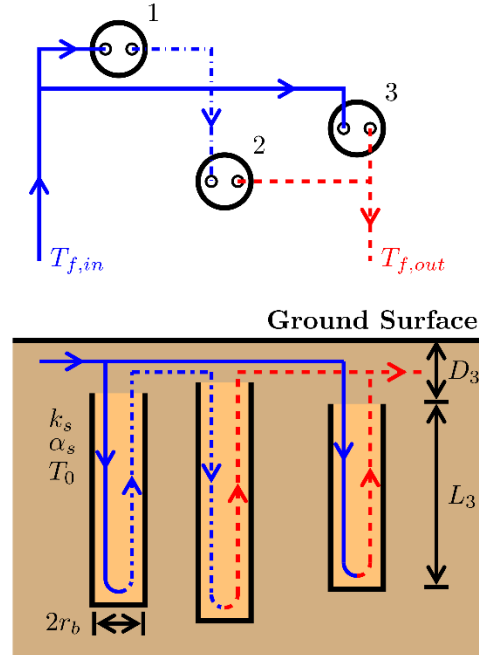


Figure 1. Field of 3 vertical geothermal boreholes

Unsteady heat conduction in the ground region

Ground temperatures in the bore field are evaluated considering heat extraction over line sources located along the axis of all of the boreholes in the field. Assuming pure conduction in semi-infinite ground with homogeneous and constant thermal properties initially at a uniform temperature T_0 with the ground surface maintained at the initial temperature T_0 , the borehole wall temperature along a borehole i is obtained by the integration of the point-source solution:

$$T_{b,i}(z_i, t) = T_0 - \sum_{j=1}^{N_b} \int_0^t \int_{D_j}^{D_j+L_j} \frac{Q'_j(z_j, t')}{\rho_s c_s [4\pi\alpha_s(t-t')]^{3/2}} \left(\exp\left(\frac{d_{ij}^2 + (z_i - z_j)^2}{4\alpha_s(t-t')}\right) - \exp\left(\frac{d_{ij}^2 + (z_i + z_j)^2}{4\alpha_s(t-t')}\right) \right) dz_j dt' \quad (3)$$

where $d_{ij} = [(x_i - x_j)^2 + (y_i - y_j)^2]^{1/2}$ is the radial (horizontal) distance between boreholes i and j , with $d_{ii} = r_{b,i}$, $z_i \in [D_i, D_i + L_i]$ is the depth along the axis of borehole i , ρ_s and c_s are density and specific heat capacity of the ground, $T_{b,i}$ is the borehole wall temperature of borehole i and Q'_j is the heat extraction rate per unit borehole length of borehole j .

Following the method of Cimmino and Bernier (2014) and Cimmino (2018c), each borehole i is divided into $n_{q,i}$ segments of equal lengths. The heat extraction rate is uniform along each of the segments and is considered constant during every time step of the simulation. The average borehole wall temperature over any borehole segment is given by spatial and temporal superpositions of the finite line source solution (Cimmino and Bernier 2014):

$$\bar{T}_{b,i,u,k} = T_0 - \frac{1}{2\pi k_s} \sum_{j=1}^{N_b} \sum_{v=1}^{n_{q,j}} \sum_{p=1}^k \bar{Q}'_{j,v,p} \left(h_{i,j,u,v}(t_k - t_{p-1}) - h_{i,j,u,v}(t_k - t_p) \right) \quad (4)$$

$$h_{i,j,u,v}(t) = \frac{1}{2L_{i,u}} \int_{\frac{1}{\sqrt{4\alpha_s t}}}^{\infty} \frac{1}{s^2} \exp(-d_{ij}^2 s^2) I_{FLS}(s) ds \quad (5)$$

$$I_{FLS}(s) = \text{erfint}\left((D_{i,u} - D_{j,v} + L_{i,u})s\right) - \text{erfint}\left((D_{i,u} - D_{j,v})s\right) + \text{erfint}\left((D_{i,u} - D_{j,v} - L_{j,v})s\right) - \text{erfint}\left((D_{i,u} - D_{j,v} + L_{i,u} - L_{j,v})s\right) + \text{erfint}\left((D_{i,u} + D_{j,v} + L_{i,u})s\right) - \text{erfint}\left((D_{i,u} + D_{j,v})s\right) + \text{erfint}\left((D_{i,u} + D_{j,v} + L_{j,v})s\right) - \text{erfint}\left((D_{i,u} + D_{j,v} + L_{i,u} + L_{j,v})s\right) \quad (6)$$

$$\text{erfint}(X) = \int_0^X \text{erf}(x') dx' = X \text{erf}(X) - \frac{1}{\sqrt{\pi}} (1 - \exp(-X^2)) \quad (7)$$

where $\bar{T}_{b,i,u,k}$ is the average borehole wall temperature along segment u of borehole i at time t_k , $\bar{Q}'_{j,v,p}$ is the average heat extraction rate per unit borehole length over segment v of borehole j from time t_{p-1} to t_p , $h_{i,j,u,v}$ is the segment-to-segment thermal response factors for the borehole wall temperature change over segment u of borehole i caused by heat extraction from segment v of borehole j , $L_{i,u} = L_i/n_{q,i}$ is the length of segment u of borehole i , $D_{i,u} = D_i + (u - 1) L_i/n_{q,i}$ is the buried depth of segment u of borehole i , $\text{erf}(x)$ is the error function and $\text{erfint}(x)$ is the integral of the error function.

It is useful at this stage to introduce the dimensionless form of Equation 1:

$$\theta_b^*(\tau) = \int_0^\tau \bar{\phi}'(\tau - \tau') \frac{dg}{d\tau}(\tau') d\tau' \quad (8)$$

where $\theta_b^* = (T_b^* - T_0)/(-Q'_{nom}/2\pi k_s)$ is the dimensionless effective borehole wall temperature in the bore field, with Q'_{nom} an arbitrary nominal heat extraction rate per unit borehole length, $\bar{\phi}' = \bar{Q}'/Q'_{nom}$ is the normalized average heat extraction rate per unit borehole length and $\tau = 9\alpha_s t/\bar{L}^2$ is the dimensionless time, with \bar{L} the average borehole length. All temperatures (e.g. fluid temperatures) may be nondimensionalized in the same manner.

The dimensionless form of Equation 4 is then:

$$\bar{\theta}_{b,i,u,k} = \sum_{j=1}^{N_b} \sum_{v=1}^{n_{q,j}} \sum_{p=1}^k \bar{\phi}'_{j,v,p} \left(h_{i,j,u,v}(\tau_k - \tau_{p-1}) - h_{i,j,u,v}(\tau_k - \tau_p) \right) \quad (9)$$

where $\bar{\theta}_{b,i,u,k}$ is the average dimensionless borehole wall temperature along segment u of borehole i at time τ_k , and $\bar{\phi}'_{j,v,p}$ is the average normalized heat extraction rate per borehole length over segment v of borehole j from time τ_{p-1} to τ_p .

Equation 9 may then be simplified by introducing matrix notation:

$$\bar{\Theta}_{b,k} = \sum_{p=1}^k \left(\mathbf{H}(\tau_k - \tau_{p-1}) - \mathbf{H}(\tau_k - \tau_p) \right) \bar{\Phi}'_p \quad (10)$$

where $\bar{\Theta}_{b,k} = [\bar{\Theta}_{b,1,k}^T \quad \cdots \quad \bar{\Theta}_{b,N_b,k}^T]^T$ is a vector of average dimensionless borehole wall temperature along all segments of all boreholes at time τ_k , $\bar{\Theta}_{b,k} = [\bar{\theta}_{b,i,1,k} \quad \cdots \quad \bar{\theta}_{b,i,n_{q,i},k}]^T$ is a vector of average borehole wall temperatures along all segments of borehole i at time τ_k , $\bar{\Phi}'_p = [\bar{\Phi}'_{1,p}^T \quad \cdots \quad \bar{\Phi}'_{N_b,p}^T]^T$ is a vector of average normalized heat extraction rates per unit borehole length along all segments of all boreholes at

time τ_p , and $\bar{\Phi}'_{j,p} = [\bar{\phi}'_{j,1,p} \quad \cdots \quad \bar{\phi}'_{j,n_{q,j},p}]^T$ is a vector of average normalized heat extraction rates per unit borehole length along all segments of borehole j at time τ_p . \mathbf{H} is a matrix of segment-to-segment thermal response factors between all pairs of segments in the bore field, given by:

$$\mathbf{H}(\tau) = \begin{bmatrix} \mathbf{H}_{1,1}(\tau) & \cdots & \mathbf{H}_{1,N_b}(\tau) \\ \vdots & \ddots & \vdots \\ \mathbf{H}_{N_b,1}(\tau) & \cdots & \mathbf{H}_{N_b,N_b}(\tau) \end{bmatrix}, \mathbf{H}_{i,j}(\tau) = \begin{bmatrix} h_{i,j,1,1}(\tau) & \cdots & h_{i,j,1,n_{q,j}}(\tau) \\ \vdots & \ddots & \vdots \\ h_{i,j,n_{q,i},1}(\tau) & \cdots & h_{i,j,n_{q,i},n_{q,j}}(\tau) \end{bmatrix} \quad (11)$$

Equation 10 is further simplified by separating the contribution of heat extraction at times preceding time τ_k from the present time τ_k :

$$\bar{\Theta}_{b,k} = \bar{\Theta}_{b,k}^0 + \mathbf{H}(\tau_k - \tau_{k-1}) \bar{\Phi}'_k \quad (12)$$

$$\bar{\Theta}_{b,k}^0 = \sum_{p=1}^{k-1} \left(\mathbf{H}(\tau_k - \tau_{p-1}) - \mathbf{H}(\tau_k - \tau_p) \right) \bar{\Phi}'_p \quad (13)$$

Quasi-steady-state heat transfer in the borehole region

Quasi-steady-state heat transfer inside the boreholes can be represented as a circuit of thermal resistances, as shown on Figure 2 for a double ($n_{p,i} = 2$) U-tube borehole. Heat transfer between the fluid flowing inside the pipes and the borehole wall is strictly two-dimensional (over the borehole cross-section); axial heat conduction in the pipes and the grout is neglected. Each borehole i has $n_{p,i}$ U-tubes ($2n_{p,i}$ pipes). Each pipe m is connected to pipe $m + n_{p,i}$ at the bottom of the borehole.

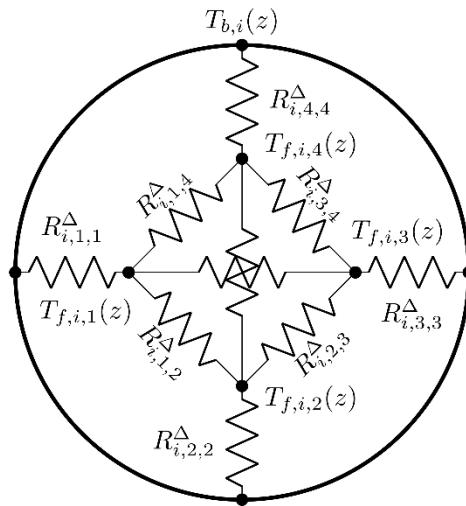


Figure 2. Delta-circuit of thermal resistances of a double U-tube borehole

Assuming steady-state heat transfer in the borehole (i.e. the thermal capacities of the fluid, pipes and grout are neglected), the fluid temperature variation along the boreholes are obtained from the following energy balance on the fluid over a borehole cross-section:

$$\dot{m}_{i,m} c_f \frac{\partial T_{f,i,m}}{\partial z}(z) = \frac{T_{f,i,m}(z) - T_{b,i}(z)}{R_{i,m,m}^\Delta} + \sum_{\substack{n=1 \\ n \neq m}}^{n_{p,i}} \frac{T_{f,i,m}(z) - T_{f,i,n}(z)}{R_{i,m,n}^\Delta}, \quad 0 \leq z \leq L_i, \quad m \leq n_{p,i} \quad (14)$$

$$-\dot{m}_{i,m} c_f \frac{\partial T_{f,i,m}}{\partial z}(z) = \frac{T_{f,i,m}(z) - T_{b,i}(z)}{R_{i,m,m}^\Delta} + \sum_{\substack{n=1 \\ n \neq m}}^{n_{p,i}} \frac{T_{f,i,m}(z) - T_{f,i,n}(z)}{R_{i,m,n}^\Delta}, \quad 0 \leq z \leq L_i, \quad n_{p,i} + 1 \leq m \leq 2n_{p,i} \quad (15)$$

where $\dot{m}_{i,m}$ is the fluid mass flow rate in pipes m and $m + n_{p,i}$, and $T_{f,i,m}$ is the fluid temperature in pipe m of borehole i . $R_{i,m,n}^\Delta$ is the delta-circuit thermal resistance between pipes m and n of borehole i and $R_{i,m,m}^\Delta$ is the delta-circuit thermal resistance between pipe m and the wall of borehole i . These delta-circuit thermal resistances can be evaluated from the multipole solution (Claesson and Hellström 2011). In this work, the multipole solution of order 3 was used to evaluate delta-circuit thermal resistances.

It is again useful to introduce dimensionless parameters by considering the dimensionless form of Equation 2:

$$\bar{\theta}_f(\tau) = \frac{1}{2}(\theta_{f,in}(\tau) + \theta_{f,out}(\tau)) = \theta_b^*(\tau) + \Omega_{field}^* \bar{\Phi}'(\tau) \quad (16)$$

where $\bar{\theta}_f$ is the dimensionless mean fluid temperature, $\theta_{f,in}$ and $\theta_{f,out}$ are the dimensionless inlet and outlet fluid temperatures of the bore field, $\Omega_{field}^* = 2\pi k_s R_{field}^*$ is the dimensionless effective bore field thermal resistance.

The dimensionless forms of Equations 14 and 15 are then:

$$\frac{\partial \theta_{f,i,m}}{\partial \eta}(\eta) = \frac{\theta_{f,i,m}(\eta) - \theta_{b,i}(\eta)}{\gamma_i \Omega_{i,m,m}^\Delta} + \sum_{\substack{n=1 \\ n \neq m}}^{n_{p,i}} \frac{\theta_{f,i,m}(\eta) - \theta_{f,i,n}(\eta)}{\gamma_i \Omega_{i,m,n}^\Delta}, \quad 0 \leq \eta \leq 1, \quad m \leq n_{p,i} \quad (17)$$

$$\frac{\partial \theta_{f,i,m}}{\partial \eta}(\eta) = \frac{\theta_{f,i,m}(\eta) - \theta_{b,i}(\eta)}{-\gamma_i \Omega_{i,m,m}^\Delta} + \sum_{\substack{n=1 \\ n \neq m}}^{n_{p,i}} \frac{\theta_{f,i,m}(\eta) - \theta_{f,i,n}(\eta)}{-\gamma_i \Omega_{i,m,n}^\Delta}, \quad 0 \leq \eta \leq 1, \quad n_{p,i} + 1 \leq m \leq 2n_{p,i} \quad (18)$$

where $\theta_{f,i,m}$ is the dimensionless fluid temperature in pipe m of borehole i , $\Omega_{i,m,n}^\Delta$ and $\Omega_{i,m,m}^\Delta$ are dimensionless delta-circuit thermal resistances, $\gamma_i = \dot{m}_i c_f / 2\pi k_s L_i$ is the dimensionless fluid mass flow rate in borehole i , and η is the normalized depth along the length of the borehole.

Equations 17 and 18 may then be simplified by introducing matrix notation:

$$\frac{\partial \boldsymbol{\Theta}_{f,i}}{\partial \eta}(\eta) = \boldsymbol{\Gamma}_i \left(\boldsymbol{\Theta}_{f,i}(\eta) - \mathbf{1}\theta_{b,i}(\eta) \right), \quad 0 \leq \eta \leq 1 \quad (19)$$

where $\boldsymbol{\Theta}_{f,i}(\eta) = [\theta_{f,i,1} \quad \cdots \quad \theta_{f,i,2n_{p,i}}]^T$ is a vector of dimensionless fluid temperatures in each pipe of borehole i , $\boldsymbol{\Gamma}_i = [\Gamma_{i,m,n}]_{2n_{p,i} \times 2n_{p,i}}$ is a dimensionless thermal conductance matrix, given by:

$$\Gamma_{i,m,n} = \begin{cases} \left(\sum_{n=1}^m (\gamma_i \Omega_{i,m,n}^\Delta) \right)^{-1} & \text{for } m = n \text{ and } m \leq n_{p,i} \\ -(\gamma_i \Omega_{i,m,n}^\Delta)^{-1} & \text{for } m \neq n \text{ and } m \leq n_{p,i} \\ -\sum_{n=1}^m (\gamma_i \Omega_{i,m,n}^\Delta)^{-1} & \text{for } m = n \text{ and } n_{p,i} + 1 \leq m \leq 2n_{p,i} \\ (\gamma_i \Omega_{i,m,n}^\Delta)^{-1} & \text{for } m \neq n \text{ and } n_{p,i} + 1 \leq m \leq 2n_{p,i} \end{cases} \quad (20)$$

The solution to Equation 19 is given by the matrix exponential (Cimmino 2016):

$$\boldsymbol{\Theta}_{f,i}(\eta) = \exp(\boldsymbol{\Gamma}_i \eta) \boldsymbol{\Theta}_{f,i}(0) - \int_0^\eta \exp(\boldsymbol{\Gamma}_i(\eta - \eta')) \boldsymbol{\Gamma}_i \mathbf{1}\theta_{b,i}(\eta') d\eta' \quad (21)$$

This solution gives the fluid temperature variation along the borehole for an arbitrary borehole wall temperature. From this solution, it is possible, considering piping connections within the borehole (series or parallel), to obtain linear relations between the inlet and outlet fluid temperatures of the borehole and between the inlet fluid temperature into the borehole and the heat extraction rate per unit length along the borehole. For a borehole i divided into $n_{q,i}$ segments of equal lengths with uniform temperature along the wall of each segment, these relations are given by:

$$\theta_{f,out,i,k} = E_{in,i}^{\theta_{out}} \theta_{f,in,i,k} + E_{b,i}^{\theta_{out}} \bar{\Theta}_{b,i,k} \quad (22)$$

$$\bar{\Phi}'_{i,k} = E_{in,i}^\phi \theta_{f,in,i,k} + E_{b,i}^\phi \bar{\Theta}_{b,i,k} \quad (23)$$

where $\theta_{f,in,i,k}$ and $\theta_{f,out,i,k}$ are the dimensionless inlet and outlet fluid temperatures of borehole i at time τ_k , and $E_{in,i}^{\theta_{out}}$, $E_{b,i}^{\theta_{out}}$, $E_{in,i}^\phi$ and $E_{b,i}^\phi$ are coefficients with values developed in appendices 1 and 2.

Piping connections in the network of boreholes

In bore fields with mixed parallel and series connections between the boreholes, the inlet fluid temperature into a borehole i may be different from the inlet fluid temperature into the bore field and is determined by the arrangement of the borehole network. The inlet fluid temperature into borehole i is either

equal to the inlet fluid temperature into the field or to the outlet fluid temperature of another borehole. The arrangement of the borehole network is represented by a borehole connectivity vector:

$$\theta_{f,\text{in},i,k} = \theta_{f,\text{out},c_{\text{in},i},k} \quad (24)$$

where $\mathbf{C}_{\text{in}} = [c_{\text{in},1} \ \cdots \ c_{\text{in},N_b}]$ is the borehole connectivity vector, with $c_{\text{in},i}$ the index of the borehole connected to the inlet of borehole i (e.g. $c_{\text{in},2} = 1$ in Figure 1); and $\theta_{f,\text{out},0,k} = \theta_{f,\text{in},k}$ is the inlet fluid temperature into the bore field (e.g. $c_{\text{in},1} = 0$ in Figure 1). For example, for the bore field represented in Figure 1, the borehole connectivity vector is $\mathbf{C}_{\text{in}} = [0 \ 1 \ 0]$. For convenience, the sequence $\mathbf{P}_{\text{in},i}$ denotes the path starting from borehole i leading to the bore field inlet. With regards to the bore field of Figure 1: $\mathbf{P}_{\text{in},1} = \{1\}$, $\mathbf{P}_{\text{in},2} = \{2,1\}$ and $\mathbf{P}_{\text{in},3} = \{3\}$.

From Equation 22 and with knowledge of the borehole connectivity, the outlet fluid temperature at any borehole can be expressed in terms of the inlet fluid temperature of the field and the borehole wall temperatures of all boreholes in its path to the inlet:

$$\theta_{f,\text{out},i,k} = \left(\prod_{j \in \mathbf{P}_{\text{in},i}} E_{\text{in},i}^{\theta_{\text{out}}} \right) \theta_{f,\text{in},k} + \sum_{j \in \mathbf{P}_{\text{in},i}} \left(\prod_{\substack{j' \in \mathbf{P}_{\text{in},i} \\ j' \neq j}} E_{\text{in},j'}^{\theta_{\text{out}}} \right) \mathbf{E}_{b,j}^{\theta_{\text{out}}} \bar{\Theta}_{b,j,k} \quad (25)$$

$$\theta_{f,\text{out},i,k} = A_{\text{in},i}^{\theta_{\text{out}}} \theta_{f,\text{in},k} + \sum_{j \in \mathbf{P}_{\text{in},i}} \mathbf{A}_{b,i,j}^{\theta_{\text{out}}} \bar{\Theta}_{b,j,k} \quad (26)$$

where $A_{\text{in},i}^{\theta_{\text{out}}}$ and $\mathbf{A}_{b,i,j}^{\theta_{\text{out}}}$ are scalar and vector coefficients, with $\mathbf{A}_{b,i,j}^{\theta_{\text{out}}} = \mathbf{0}$ if $j \notin \mathbf{P}_{\text{in},i}$, Π is the product operator, with $\prod_{j \in \{1,2,3\}} E_{\text{in},i}^{\theta_{\text{out}}} = E_{\text{in},1}^{\theta_{\text{out}}} E_{\text{in},2}^{\theta_{\text{out}}} E_{\text{in},3}^{\theta_{\text{out}}}$ and $\prod_{j \in \{\}} E_{\text{in},i}^{\theta_{\text{out}}} = 1$.

From Equations 23 and 25, and considering the borehole connectivity, the heat extraction rate per unit borehole length of any borehole may also be expressed in terms of the inlet fluid temperature of the field and the borehole wall temperatures of all boreholes in its path to the inlet:

$$\bar{\Phi}'_{i,k} = \mathbf{E}_{\text{in},i}^{\phi} \left(\prod_{\substack{j \in \mathbf{P}_{\text{in},i} \\ j \neq i}} E_{\text{in},j}^{\theta_{\text{out}}} \right) \theta_{f,\text{in},k} + \sum_{j \in \mathbf{P}_{\text{in},i}} \left(\prod_{\substack{j' \in \mathbf{P}_{\text{in},i} \\ j' \neq j}} E_{\text{in},j'}^{\theta_{\text{out}}} \right) \mathbf{E}_{b,j}^{\phi} \bar{\Theta}_{b,j,k} \quad (27)$$

$$\bar{\Phi}'_{i,k} = \mathbf{A}_{\text{in},i}^{\phi} \theta_{f,\text{in},k} + \sum_{j \in \mathbf{P}_{\text{in},i}} \mathbf{A}_{b,i,j}^{\phi} \bar{\Theta}_{b,j,k} \quad (28)$$

where $\mathbf{A}_{\text{in},i}^{\phi}$ and $\mathbf{A}_{b,i,j}^{\phi}$ are vector and matrix coefficients, with $\mathbf{A}_{b,i,j}^{\phi} = \mathbf{0}$ if $j \notin \mathbf{P}_{\text{in},i}$.

The heat extraction rates per unit borehole length of all borehole segments are then given by assembling Equation 28 for all boreholes in the field:

$$\bar{\Phi}'_k = \mathbf{A}_{\text{in}}^\phi \theta_{f,\text{in},k} + \mathbf{A}_b^\phi \bar{\Theta}_{b,k} \quad (29)$$

$$\mathbf{A}_{\text{in}}^\phi = \begin{bmatrix} \mathbf{A}_{\text{in},1}^\phi \\ \vdots \\ \mathbf{A}_{\text{in},N_b}^\phi \end{bmatrix} \quad (30)$$

$$\mathbf{A}_b^\phi = \begin{bmatrix} \mathbf{A}_{b,1,1}^\phi & \cdots & \mathbf{A}_{b,1,N_b}^\phi \\ \vdots & \ddots & \vdots \\ \mathbf{A}_{b,N_b,1}^\phi & \cdots & \mathbf{A}_{b,N_b,N_b}^\phi \end{bmatrix} \quad (31)$$

The outlet fluid temperature of the bore field is obtained by an energy balance:

$$\theta_{f,\text{out},k} = \theta_{f,\text{in},k} - N_b \frac{\bar{\Phi}'_k}{\gamma} \quad (32)$$

$$\theta_{f,\text{out},k} = \left(1 - \frac{1}{\gamma} \mathbf{L} \mathbf{A}_{\text{in}}^\phi\right) \theta_{f,\text{in},k} - \frac{1}{\gamma} \mathbf{L} \mathbf{A}_b^\phi \bar{\Theta}_{b,k} \quad (33)$$

$$\theta_{f,\text{out},k} = \mathbf{A}_{\text{in}}^{\theta_{\text{out}}} \theta_{f,\text{in},k} + \mathbf{A}_b^{\theta_{\text{out}}} \bar{\Theta}_{b,k} \quad (34)$$

where $\gamma = \dot{m} c_f / 2\pi k_s \bar{L}$ is the dimensionless total fluid mass flow rate, $\bar{\Phi}'_k = \mathbf{L} \bar{\Phi}'_k / N_b \bar{L}$ is the normalized average heat extraction rate per unit borehole length in the bore field, $\mathbf{L} = [\mathbf{L}_1 \quad \cdots \quad \mathbf{L}_{N_b}]$ is a vector of the lengths of all borehole segments in the bore field, with $\mathbf{L}_i = [L_{i,1} \quad \cdots \quad L_{i,n_{q,i}}]$.

g-Function of the bore field

Dimensionless borehole wall and inlet fluid temperatures

Per the definition of the g-function (Equations 1 and 8), the g-function is obtained from the dimensionless borehole wall temperature response to a constant unit normalized heat extraction rate per borehole length:

$$\bar{\Phi}'_k = \mathbf{L} \bar{\Phi}'_k / N_b \bar{L} = 1 \quad (35)$$

The dimensionless borehole wall and inlet fluid temperature responses are obtained by the simultaneous solution of Equations 12, 29 and 35:

$$\begin{bmatrix} \mathbf{H}(\tau_k - \tau_{k-1}) & -\mathbf{I} & \mathbf{0} \\ -\mathbf{I} & \mathbf{A}_b^\phi & \mathbf{A}_{in}^\phi \\ \mathbf{L}/N_b\bar{L} & \mathbf{0} & 0 \end{bmatrix} \begin{bmatrix} \bar{\Phi}'_k \\ \bar{\Theta}_{b,k} \\ \theta_{f,in,k} \end{bmatrix} = \begin{bmatrix} -\bar{\Theta}_{b,k}^0 \\ \mathbf{0} \\ 1 \end{bmatrix} \quad (36)$$

where \mathbf{I} is the identity matrix.

Effective borehole and bore field thermal resistances

To evaluate the effective dimensionless borehole wall temperature – and thus the g -function – the effective bore field thermal resistance (defined by Equations 2 and 16) must first be evaluated. The concept of effective borehole thermal resistance was first introduced by Hellström (1991), who considered a uniform borehole wall temperature and obtained the effective borehole thermal resistance based on the arithmetic mean fluid temperature:

$$\Omega_{b,i}^* = \frac{\frac{1}{2}(\theta_{f,in,i,k} + \theta_{f,out,i,k}) - \theta_{b,i,k}^*}{\bar{\Phi}'_{i,k}} \quad (37)$$

where $\bar{\Phi}'_{i,k} = \mathbf{L}_i \bar{\Phi}'_{i,k} / L_i$ is the average normalized heat extraction rate per unit length of borehole i , $\theta_{b,i,k}^*$ is the effective uniform dimensionless borehole wall temperature of borehole i , and $\Omega_{b,i}^* = 2\pi k_s R_{b,i}^*$ is the effective dimensionless borehole thermal resistance of borehole i .

From Equations 22 and 23 and assuming a zero dimensionless borehole wall temperature, $\theta_{b,i,k}^* = 0$:

$$\Omega_{b,i}^* = \frac{1}{2} \cdot \frac{1 + E_{in,i}^{\theta_{out}}}{\mathbf{L}_i E_{in,i}^\phi / L_i} \quad (38)$$

Similarly, the bore field thermal resistance is defined as the ratio of the temperature difference between the arithmetic mean fluid temperature in the bore field and the effective borehole wall temperature, and the average heat extraction rate per unit borehole length in the bore field, considering a uniform *effective* borehole wall temperature across the bore field:

$$\Omega_{field}^* = \frac{\frac{1}{2}(\theta_{f,in,k} + \theta_{f,out,k}) - \theta_{b,k}^*}{\bar{\Phi}'_k} \quad (39)$$

From Equations 29 and 34 and assuming a zero dimensionless borehole wall temperature, $\theta_{b,i,k}^* = 0$:

$$\Omega_{field}^* = \frac{1}{2} \cdot \frac{1 + A_{in}^{\theta_{out}}}{\mathbf{L} A_{in}^\phi / N_b \bar{L}} \quad (40)$$

Effective dimensionless borehole wall temperature

The solution of Equation 36 gives the variation of the dimensionless inlet fluid temperature into the bore field. From Equations 16 and 32, the effective dimensionless borehole wall temperature is given by:

$$\theta_b^*(\tau_k) = \theta_{f,in,k} - \frac{N_b}{2\gamma} - \Omega_{field}^* \quad (41)$$

where θ_b^* is the effective dimensionless borehole wall temperature, equal to the g -function of the bore field. In combination with the effective bore field thermal resistance, the g -function permits the simulation of fluid temperatures in geothermal bore fields with series- and parallel-connected boreholes. An example of the complete calculation process for the evaluation of the g -function of a field of 2 series-connected boreholes is detailed in Appendix 3.

Results

A field of 144 boreholes is shown on Figure 3. The field consists of 24 parallel branches of 6 series-connected single U-tube boreholes of equal dimensions. The dimensional and physical parameters of the bore field are presented in Table 1. Fluid enters the 24 parallel branches from the center of the field and exits from its perimeter. The fluid mass flow rate is evenly distributed across all branches. The effective borehole thermal resistance is $R_b^* = 0.1460$ m-K/W, corresponding to a dimensionless effective borehole thermal resistance of $\Omega_b^* = 1.835$. The effective bore field thermal resistance is $R_{field}^* = 0.1700$ m-K/W, corresponding to a dimensionless effective borehole thermal resistance of $\Omega_{field}^* = 2.136$. The dimensionless total fluid mass flow rate is $\gamma = 54.25$. With regards to the number of boreholes, the number of parallel branches, the length of the boreholes and the average spacing between the boreholes, the bore field in Figure 3 is similar to the borehole thermal energy storage of Drake Landing Solar Community (Sibbitt et al. 2012). In this section, the presented g -function calculation method is compared to the results of simulations obtained using the duct ground heat storage (DST) model (Pahud and Hellström 1996). The effect of fluid mass flow rate on the g -function and on the effective bore field thermal resistance is then studied.

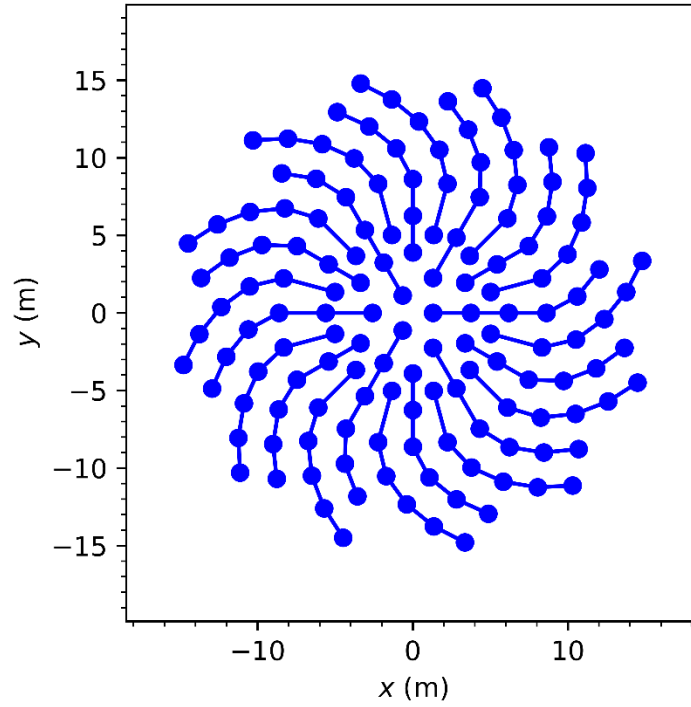


Figure 3. Bore field of 144 boreholes in 24 parallel branches of 6 series-connected boreholes

Table 1. Parameters of the bore field		
Parameter	Value	Units
Bore field		
Number of boreholes, N_b	144	-
Number of parallel branches	24	-
Boreholes per branch	6	-
Nominal borehole spacing	2.25	m
Total fluid mass flow rate, \dot{m}	6	kg/s
Boreholes		
Borehole length, L	35	m
Borehole radius, r_b	0.075	m
Borehole buried depth, D	0.5	m
Piping		
Number of U-tubes per borehole, n_p	1	-
Pipe outer diameter	0.0422	m
Pipe inner diameter	0.0294	m
Shank spacing	0.052	m
Pipe surface roughness	10^{-6}	m
Physical properties		
Undisturbed ground temperature, T_0	10	°C
Ground thermal conductivity, k_s	2	W/m-K
Ground thermal diffusivity, α_s	10^{-6}	m ² /s
Grout thermal conductivity	1	W/m-K
Pipe thermal conductivity	0.4	W/m-K
Fluid thermal conductivity	0.492	W/m-K
Fluid density	1015	kg/m ³
Fluid specific heat capacity, c_f	3977	J/kg-K
Fluid dynamic viscosity	0.00203	kg/m-s

g-Function of the bore field

The effective dimensionless borehole wall temperature (i.e. the g -function) and the dimensionless inlet fluid temperature obtained from the presented methodology are shown on Figure 4, using $n_q = 12$ segments per borehole. The dimensionless temperatures are compared to the average storage temperature and the inlet fluid temperature obtained from a constant heat injection simulation using the DST model. As the DST model does not consider the positions of the boreholes in the bore field, but rather assumes evenly distributed boreholes in a specified storage volume, a storage volume of 25,270 m³ given by the cylindrical volume delimited by the boreholes furthest from the center of the field was used for this simulation. The simulation was performed with a time step of 1 hour over a simulation period of 100 years and a constant heat injection rate $\bar{Q}' = 2\pi k_S$. The effective borehole wall temperature is not directly comparable to the average storage temperature, as the former is representative of the temperature in the immediate vicinity of the boreholes while the latter is representative of the average temperature in the volume. For this reason, the inlet fluid temperatures are better suited for comparison between the g -function and the DST model (Pahud and Hellström 1996). The results are close, with a maximum absolute difference of 1.46 at $\ln(\tau) = 1.8$ when the dimensionless inlet fluid temperature is 54.02, and a maximum relative difference of 4.2 % at $\ln(\tau) = -9.9$ corresponding to the second time step of the DST simulation. Differences are expected since the DST model does not consider the actual positions of the boreholes.

The calculation time for the evaluation of the g -function of the field of 144 boreholes over 100 time steps using $n_q = 12$ segments per borehole is 447 seconds on a computer equipped with a 4.2 GHz quad core (8 threads) processor. Comparatively, the calculation time for the evaluation of the g -function of the same bore field using a uniform borehole wall temperature condition as per the method of Cimmino and Bernier (2014) and Cimmino (2018c) (i.e. without consideration for the fluid temperature variations and the connections between boreholes) is 412 seconds. The time difference is caused by the increased size of the system of equations solved in Equation 36, as the time required for the evaluation of the matrix of segment-to-segment thermal response factors, \mathbf{H} , is 220 seconds in both cases.

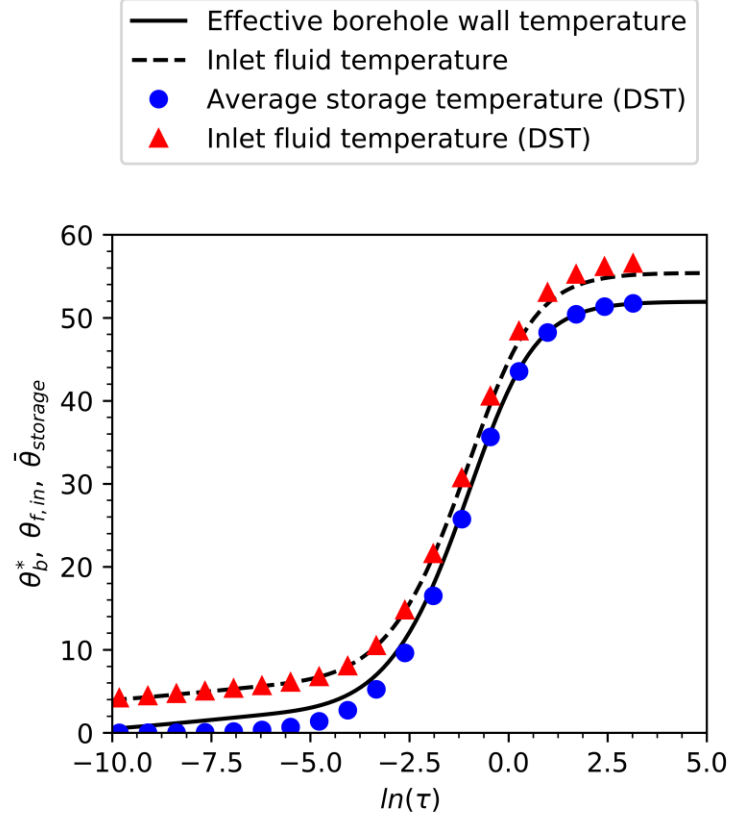


Figure 4. Comparison of the dimensionless effective borehole wall and inlet fluid temperatures with the DST model

Simulation of a seasonal storage system

The g -function of the bore field presented in Figure 4 is used in a sample simulation of a seasonal thermal energy storage system. Simplified relations are used for the total heat extraction from the bore field, given as the sum of heat extraction due to building heating loads and solar thermal collectors (heat injection corresponds to negative heat extraction). The building heating loads, $Q_{buildings}$, are represented by a linear relation with ambient temperature:

$$Q_{buildings} = \max(0, -7500[W/K] \cdot T_{amb} + 75000[W]) \quad (42)$$

where T_{amb} is the ambient temperature (in °C), averaged over the 6 preceding hours, obtained from a typical meteorological year for the city of Montreal, Canada (Numerical Logics 1999). In the simulation,

solar heat injection started at the beginning of the system's operation, on January 1st, while building heating loads were only applied at the beginning of the following heating season, in September of the first year.

The heat extraction rate from solar collectors is given by:

$$Q_{solar} = -A_{col}\eta G \quad (43)$$

where $A_{col} = 750 \text{ m}^2$ is the total solar collector area, $\eta = 0.6$ is a constant solar collector efficiency and G is the total solar radiation on solar collectors facing due south with a slope of 45° , obtained for the same typical meteorological year.

A 5 year simulation of the seasonal thermal storage system was conducted with the DST model with a time step of 1 hour. Using the same ground heat extraction rates, the effective borehole wall temperature were obtained from the temporal superposition of the g -function, using the FFT technique proposed by Marcotte and Pasquier (2008). The inlet fluid temperatures were then obtained from Equation 2. The inlet fluid temperatures during the 5th simulation year predicted from the temporal superposition of the g -function are presented on Figure 5, along with the average heat extraction rate per unit borehole length. Predicted inlet fluid temperatures are in good agreement with the DST model, as shown on Figure 6 for a 5 day period of the 5th simulation year, starting on June 30th. This 5 day period coincides with the maximum difference of $1.85 \text{ }^\circ\text{C}$ between the inlet temperatures predicted by the two models.

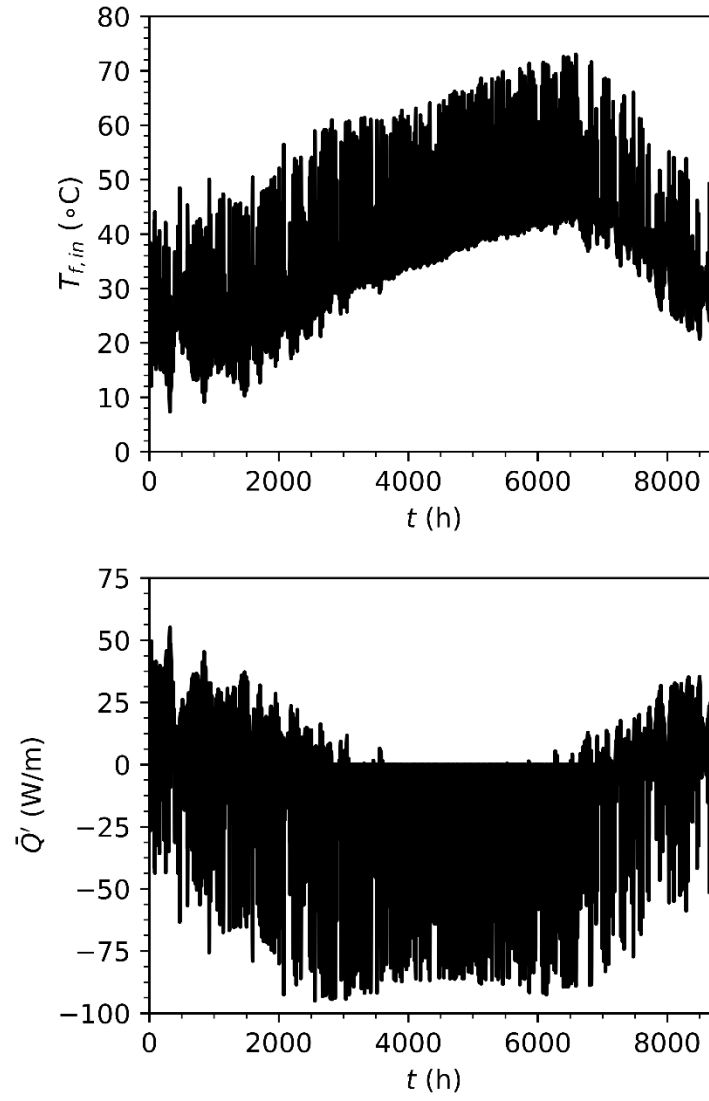


Figure 5. Inlet fluid temperature during the 5th simulation year (above), and average heat extraction rate per unit borehole length (below)

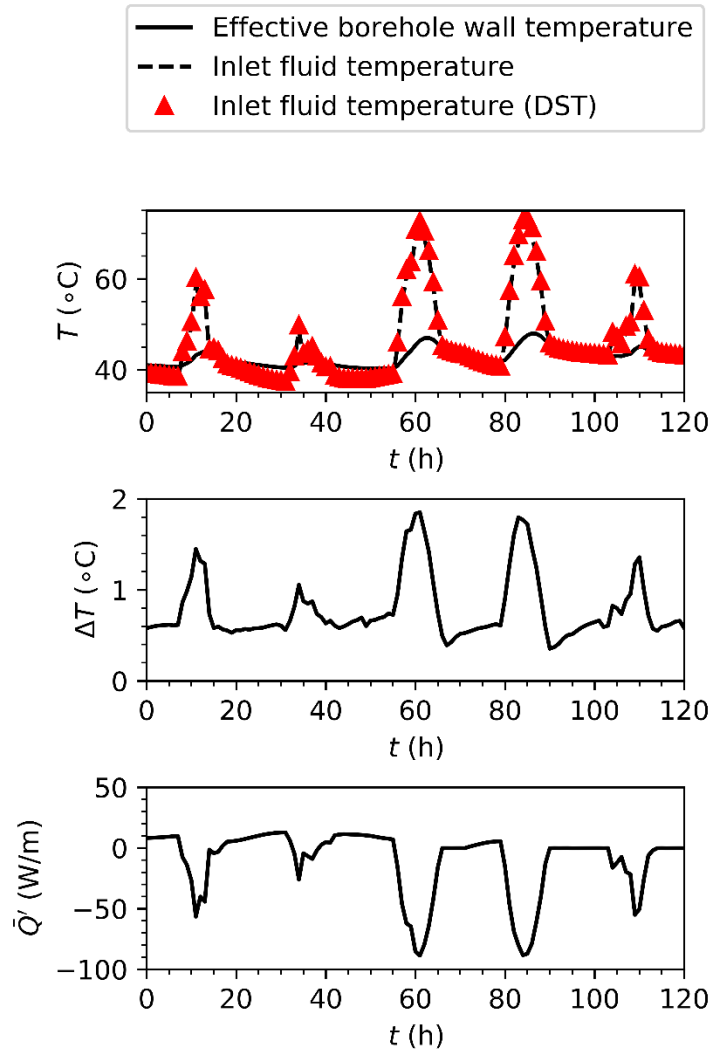


Figure 6. Comparison of the inlet fluid temperatures predicted by the g -function and the DST model (above), difference between the two models (center), and average heat extraction rate per unit borehole length (below)

Fluid mass flow rate

The influence of the fluid mass flow rate on the g -function is presented on Figure 7. It is shown that the difference between the inlet fluid temperature and the effective borehole wall temperature increases when the mass flow rate is reduced, as predicted by Equation 41. It is also shown that, for sufficiently large mass flow rates, the effective dimensionless borehole wall temperature does not show significant variations. At

$\ln(\tau) = 5$, the values of the effective dimensionless borehole wall temperature are 51.5 and 52.0 for dimensionless fluid mass flow rates of $\gamma = 25$ and 125, respectively. These results imply that, for sufficiently large mass flow rates, the same g -function can be used for simulation. The effect of the fluid mass flow rate is further demonstrated on Figure 8, comparing the steady-state dimensionless inlet fluid temperature and effective dimensionless borehole wall temperature at varying mass flow rates. For the bore field of Figure 3, the steady-state effective borehole wall temperature only varies by 1 % for $\gamma \geq 21.8$. The sharp variation around $\ln(\tau) = 3$ is due to the transition from laminar to turbulent flow within the boreholes. The variations of the effective dimensionless borehole wall temperature are explained by the variations of the effective bore field thermal resistance, as shown on Figure 9. In the same range $\gamma \geq 21.8$, the effective bore field thermal resistance varies from 4.07 to 1.76. These results are in agreement to that of Cimmino (2015) who found that, for parallel-connected boreholes, the values of the g -function depend on the effective borehole thermal resistance. It should be noted that, for infinite mass flow rate (i.e. $\gamma \rightarrow \infty$), the effective bore field thermal resistance (defined in Equation 2) tends to the same value as the effective borehole thermal resistance.

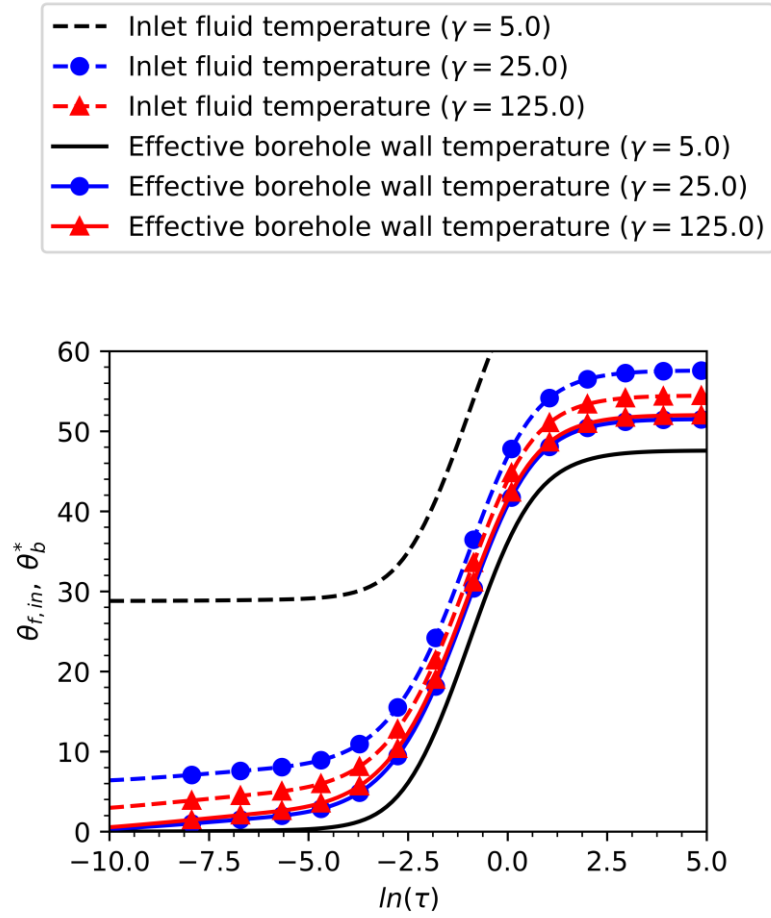


Figure 7. Influence of the dimensionless fluid mass flow rate on the dimensionless inlet fluid temperature and on the effective dimensionless borehole wall temperature

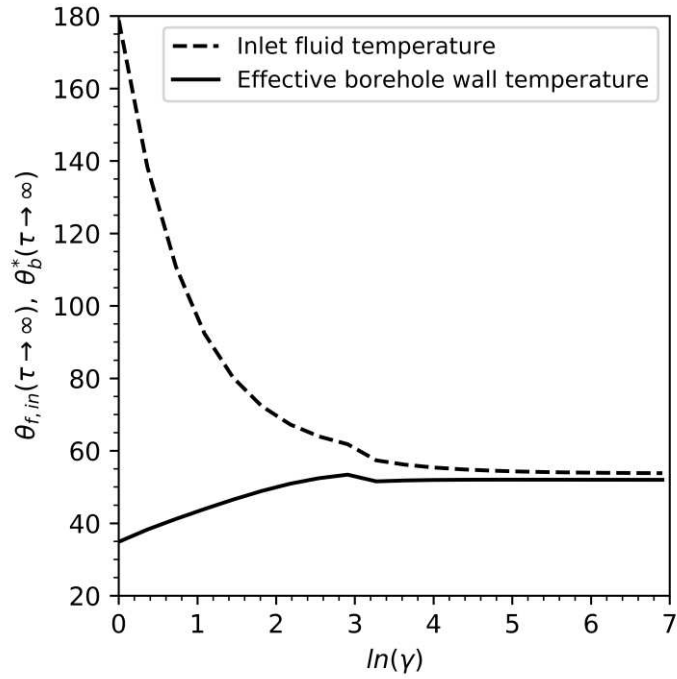


Figure 8. Influence of the dimensionless fluid mass flow rate on the steady-state dimensionless effective borehole wall temperature and on the steady-state dimensionless inlet fluid temperature

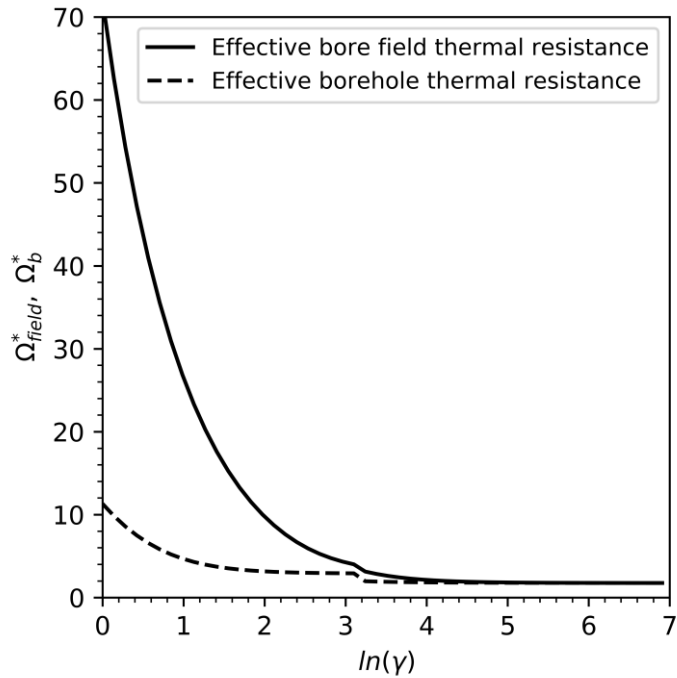


Figure 9. Influence of the dimensionless fluid mass flow rate on the effective borehole thermal resistance and the effective bore field thermal resistance

Conclusion

A semi-analytical method for the calculation of g -functions of bore fields with mixed arrangements of series- and parallel-connected boreholes is presented. Borehole wall temperature variations are obtained from the temporal and spatial superposition of the finite line source solution. Heat transfer between the fluid and the borehole wall is obtained from an analytical solution based on an energy balance on a thermal resistance network representing a borehole cross-section. The concept of effective bore field thermal resistances is introduced and is used in the definition of the effective borehole wall temperature. This yields a linear relation between the arithmetic mean fluid temperature, the heat extraction rate per unit borehole length and the effective bore field thermal resistance, as is typically encountered in simulations of parallel-connected borehole fields.

The g -function calculation method is validated against the DST model on a bore field consisting of 24 parallel branches of 6 series-connected boreholes, totalling 144 boreholes. Some small differences in predicted inlet fluid temperatures are observed but can be explained by the fundamental differences between the two methods, i.e. the positions of the boreholes are not explicitly prescribed in the DST model. The g -function is shown to be dependent on the fluid mass flow rate, although variations in g -function values are not significant at sufficiently high fluid mass flow rates. An important limitation of the proposed method is that it is not possible to account for changes in flow direction within the bore field, which can be expected in seasonal storage systems. This limitation will be addressed in future work.

Nomenclature

A, \mathbf{A} : Coefficient, vector of coefficients or matrix of coefficients
 \mathbf{C}_{in} : Borehole connectivity vector
 c_f : Fluid specific heat capacity, J/kg-K
 D : Buried depth, m
 d : Distance, m
 E, \mathbf{E} : Coefficient, vector of coefficients or matrix of coefficients
 G : Total incident solar radiation
 g : g -function
 \mathbf{H} : Matrix of segment-to-segment thermal response factors
 h : Segment-to-segment thermal response factor
 I_{FLS} : Axial portion of the integrand function of the finite line source solution
 k : Thermal conductivity, W/m-K
 L : Length, m

\dot{m} : Mass flow rate, kg/s
 N_b : Number of boreholes
 n_p : Number of U-tubes
 n_q : Number of borehole segments
 \mathbf{P}_{in} : Path sequence to bore field inlet
 Q : Heat extraction rate, W
 Q' : Heat extraction rate per unit length, W/m
 R : Thermal resistance, m-K/W
 r : Radius, m
 T : Temperature, °C
 t : Time, s
 (x, y) : Borehole horizontal coordinates, m
 \mathbf{Y} : Vector of dimensionless fluid mass flow rates
 z : Vertical coordinate, m

Greek symbols

α : Thermal diffusivity, m²/s
 $\mathbf{\Gamma}$: Dimensionless thermal conductance matrix
 γ : Dimensionless fluid mass flow rate
 η : Dimensionless vertical coordinate
 $\mathbf{\Theta}$: Vector of dimensionless temperatures
 θ : Dimensionless temperature
 ρ : Density, kg/m³
 τ : Dimensionless time
 $\mathbf{\Phi'}$: Vector of dimensionless heat extraction rates per unit length
 ϕ' : Dimensionless heat extraction rate per unit length
 Ω : Dimensionless thermal resistance

Subscripts

0 : Initial
 b : Borehole, or borehole wall (temperature)
 f : Fluid
 $field$: Bore field
 i, j : Borehole indices
 in : Inlet
 k, p : Time step indices
 m, n : Pipe indices
 nom : Nominal value
 out : Outlet
 s : Soil
 $storage$: Storage (DST model)
 u, v : Borehole segment indices

Superscripts

()^{*} : Effective value

()^Δ : Delta-circuit

References

- Abdelaziz, S. L., T. Y. Ozudogru, C. G. Olgun, and J. R. Martin. 2014. "Multilayer Finite Line Source Model for Vertical Heat Exchangers." *Geothermics* 51: 406–416.
doi:10.1016/j.geothermics.2014.03.004.
- ASHRAE. 2015. *ASHRAE Handbook — HVAC Applications*. Atlanta GA, USA: American Society of Heating, Refrigerating and Air Conditioning Engineers.
- Bandyopadhyay, G., W. Gosnold, and M. Mann. 2008. "Analytical and Semi-Analytical Solutions for Short-Time Transient Response of Ground Heat Exchangers." *Energy and Buildings* 40 (10). Elsevier: 1816–1824. doi:10.1016/J.ENBUILD.2008.04.005.
- Beier, R. A., and M. D. Smith. 2003. "Minimum Duration of In-Situ Tests on Vertical Boreholes." *ASHRAE Transactions* 109: 475–486.
- Cimmino, M. 2015. "The Effects of Borehole Thermal Resistances and Fluid Flow Rate on the G-Functions of Geothermal Bore Fields." *International Journal of Heat and Mass Transfer* 91: 1119–1127. doi:10.1016/j.ijheatmasstransfer.2015.08.041.
- Cimmino, M. 2016. "Fluid and Borehole Wall Temperature Profiles in Vertical Geothermal Boreholes with Multiple U-Tubes." *Renewable Energy* 96: 137–147. doi:10.1016/j.renene.2016.04.067.
- Cimmino, M. 2018a. "A Finite Line Source Simulation Model for Geothermal Systems with Series- and Parallel-Connected Boreholes and Independent Fluid Loops." *Journal of Building Performance Simulation* 11 (4): 414–432. doi:10.1080/19401493.2017.1381993.
- Cimmino, M. 2018b. "G-Functions for Bore Fields with Mixed Parallel and Series Connections Considering Axial Fluid Temperature Variations." In *Proceedings of the IGSHPA Research Track 2018*, 262–270. International Ground Source Heat Pump Association.
doi:10.22488/okstate.18.000015.
- Cimmino, M. 2018c. "Fast Calculation of the G-Functions of Geothermal Borehole Fields Using Similarities in the Evaluation of the Finite Line Source Solution." *Journal of Building Performance Simulation* 11 (6): 655–668. doi:10.1080/19401493.2017.1423390.
- Cimmino, M., and M. Bernier. 2014. "A Semi-Analytical Method to Generate g-Functions for Geothermal Bore Fields." *International Journal of Heat and Mass Transfer* 70 (c): 641–650.
doi:10.1016/j.ijheatmasstransfer.2013.11.037.
- Cimmino, M., M. Bernier, and F. Adams. 2013. "A Contribution towards the Determination of G-Functions Using the Finite Line Source." *Applied Thermal Engineering* 51 (1–2): 401–412.
doi:10.1016/j.applthermaleng.2012.07.044.
- Claesson, J., and G. Hellström. 2011. "Multipole Method to Calculate Borehole Thermal Resistances in a Borehole Heat Exchanger." *HVAC&R Research* 17 (6): 895–911.
doi:10.1080/10789669.2011.609927.
- Claesson, J., and S. Javed. 2011. "An Analytical Method to Calculate Borehole Fluid Temperatures for Time-Scales from Minutes to Decades." *ASHRAE Transactions* 117 (2): 279–288.
- Cui, P., H. Yang, and Z. Fang. 2006. "Heat Transfer Analysis of Ground Heat Exchangers with Inclined Boreholes." *Applied Thermal Engineering* 26 (11–12): 1169–1175.
doi:10.1016/j.applthermaleng.2005.10.034.
- Dusseault, B., P. Pasquier, and D. Marcotte. 2018. "A Block Matrix Formulation for Efficient G-Function Construction." *Renewable Energy* 121 (June). Pergamon: 249–260.
doi:10.1016/J.RENENE.2017.12.092.
- Erol, S., and B. François. 2018. "Multilayer Analytical Model for Vertical Ground Heat Exchanger with Groundwater Flow." *Geothermics* 71 (January). Pergamon: 294–305.
doi:10.1016/J.GEOTHERMICS.2017.09.008.

- Eskilson, P. 1987. "Thermal Analysis of Heat Extraction Boreholes." University of Lund.
- Fossa, M. 2011. "The Temperature Penalty Approach to the Design of Borehole Heat Exchangers for Heat Pump Applications." *Energy and Buildings* 43 (6): 1473–1479. doi:10.1016/j.enbuild.2011.02.020.
- Hellström, G. 1991. "Ground Heat Storage: Thermal Analysis of Duct Storage Systems." University of Lund.
- Hu, J. 2017. "An Improved Analytical Model for Vertical Borehole Ground Heat Exchanger with Multiple-Layer Substrates and Groundwater Flow." *Applied Energy* 202 (September): 537–549. doi:10.1016/j.apenergy.2017.05.152.
- Javed, S., and J. Claesson. 2011. "New Analytical and Numerical Solutions for the Short-Term Analysis of Vertical Ground Heat Exchangers." *ASHRAE Transactions* 117: 279–288.
- Lamarche, L. 2011. "Analytical G-Function for Inclined Boreholes in Ground-Source Heat Pump Systems." *Geothermics* 40 (4): 241–249. doi:10.1016/j.geothermics.2011.07.006.
- Lamarche, L., and B. Beauchamp. 2007a. "A New Contribution to the Finite Line-Source Model for Geothermal Boreholes." *Energy and Buildings* 39 (2): 188–198. doi:10.1016/j.enbuild.2006.06.003.
- Lamarche, L., and B. Beauchamp. 2007b. "New Solutions for the Short-Time Analysis of Geothermal Vertical Boreholes." *International Journal of Heat and Mass Transfer* 50 (7–8). Pergamon: 1408–1419. doi:10.1016/J.IJHEATMASSTRANSFER.2006.09.007.
- Lamarche, L. 2015. "Short-Time Analysis of Vertical Boreholes, New Analytic Solutions and Choice of Equivalent Radius." *International Journal of Heat and Mass Transfer* 91 (December): 800–807. doi:10.1016/j.ijheatmasstransfer.2015.07.135.
- Lamarche, L. 2017a. "Mixed Arrangement of Multiple Input-Output Borehole Systems." *Applied Thermal Engineering*. doi:10.1016/j.applthermaleng.2017.06.060.
- Lamarche, L. 2017b. "G-Function Generation Using a Piecewise-Linear Profile Applied to Ground Heat Exchangers." *International Journal of Heat and Mass Transfer* 115 (December): 354–360. doi:10.1016/j.ijheatmasstransfer.2017.08.051.
- Lazzarotto, A. 2014. "A Network-Based Methodology for the Simulation of Borehole Heat Storage Systems." *Renewable Energy* 62: 265–275. doi:10.1016/j.renene.2013.07.020.
- Lazzarotto, A. 2016. "A Methodology for the Calculation of Response Functions for Geothermal Fields with Arbitrarily Oriented Boreholes – Part 1." *Renewable Energy* 86: 1380–1393. doi:10.1016/j.renene.2015.09.056.
- Li, M., and A. C. K. Lai. 2012a. "New Temperature Response Functions (G Functions) for Pile and Borehole Ground Heat Exchangers Based on Composite-Medium Line-Source Theory." *Energy* 38 (1). Pergamon: 255–263. doi:10.1016/J.ENERGY.2011.12.004.
- Li, M., and A. C. K. Lai. 2012b. "Heat-Source Solutions to Heat Conduction in Anisotropic Media with Application to Pile and Borehole Ground Heat Exchangers." *Applied Energy* 96 (August): 451–458. doi:10.1016/j.apenergy.2012.02.084.
- Li, M., and A. C. K. Lai. 2013. "Analytical Model for Short-Time Responses of Ground Heat Exchangers with U-Shaped Tubes: Model Development and Validation." *Applied Energy* 104 (April). Elsevier: 510–516. doi:10.1016/J.APENERGY.2012.10.057.
- Marcotte, D., and P. Pasquier. 2008. "Fast Fluid and Ground Temperature Computation for Geothermal Ground-Loop Heat Exchanger Systems." *Geothermics* 37 (6): 651–665. doi:10.1016/j.geothermics.2008.08.003.
- Marcotte, D., and P. Pasquier. 2009. "The Effect of Borehole Inclination on Fluid and Ground Temperature for GLHE Systems." *Geothermics* 38 (4): 392–398. doi:10.1016/j.geothermics.2009.06.001.
- Marcotte, D., and P. Pasquier. 2014. "Unit-Response Function for Ground Heat Exchanger with Parallel, Series or Mixed Borehole Arrangement." *Renewable Energy* 68: 14–24. doi:10.1016/j.renene.2014.01.023.
- Molina-Giraldo, N., P. Blum, K. Zhu, P. Bayer, and Z. Fang. 2011. "A Moving Finite Line Source Model to Simulate Borehole Heat Exchangers with Groundwater Advection." *International Journal of Thermal Sciences* 50 (12): 2506–2513. doi:10.1016/j.ijthermalsci.2011.06.012.
- Monzó, P., P. Mogensen, J. Acuña, F. Ruiz-Calvo, and C. Montagud. 2015. "A Novel Numerical Approach for Imposing a Temperature Boundary Condition at the Borehole Wall in Borehole Fields." *Geothermics* 56 (July). Pergamon: 35–44. doi:10.1016/J.GEOTHERMICS.2015.03.003.
- Monzó, P., A. R. Puttige, J. Acuña, P. Mogensen, A. Cazorla, J. Rodriguez, C. Montagud, and F. Cerdeira.

2018. “Numerical Modeling of Ground Thermal Response with Borehole Heat Exchangers Connected in Parallel.” *Energy and Buildings* 172 (August). Elsevier: 371–384. doi:10.1016/J.ENBUILD.2018.04.057.
- Naldi, C., and E. Zanchini. 2019. “A New Numerical Method to Determine Isothermal G-Functions of Borehole Heat Exchanger Fields.” *Geothermics* 77 (January). Pergamon: 278–287. doi:10.1016/J.GEOTHERMICS.2018.10.007.
- Numerical Logics. 1999. “Canadian Weather for Energy Calculations, Users Manual and CD-ROM.” Downsview ON, Canada: Environment Canada.
- Pahud, D., and G. Hellström. 1996. “The New Duct Ground Heat Model for TRNSYS.” In *Proceedings of Eurotherm Seminar N° 49*, edited by A. A. van Steenhoven and W. G. J. van Helden, 127–136. Eindhoven, The Netherlands.
- Sibbitt, B., D. McClenahan, R. Djebbar, J. Thornton, B. Wong, J. Carriere, and J. Kokko. 2012. “The Performance of a High Solar Fraction Seasonal Storage District Heating System – Five Years of Operation.” *Energy Procedia* 30 (January). Elsevier: 856–865. doi:10.1016/J.EGYPRO.2012.11.097.
- Zeng, H. Y., N. R. Diao, and Z. H. Fang. 2002. “A Finite Line-Source Model for Boreholes in Geothermal Heat Exchangers.” *Heat Transfer - Asian Research* 31 (7): 558–567. doi:10.1002/htj.10057.

Appendix 1 : Coefficients for the evaluation of fluid temperatures

The solution to Equation 19 gives the fluid temperature variation in each of the pipes inside a borehole:

$$\Theta_{f,i}(\eta) = \exp(\Gamma_i \eta) \Theta_{f,i}(0) - \int_0^\eta \exp(\Gamma_i(\eta - \eta')) \Gamma_i \mathbf{1}\theta_{b,i}(\eta') d\eta' \quad (44)$$

where $\Theta_{f,i}(0)$ is a vector of fluid temperature in each of the pipes at the top of borehole i .

For a borehole i divided into $n_{q,i}$ segments of equal lengths with uniform borehole wall temperature along each of the segments:

$$\Theta_{f,i}(\eta) = \exp(\Gamma_i \eta) \Theta_{f,i}(0) + \sum_{u=1}^{n_{q,i}} \Gamma_i^{-1} [\exp(\Gamma_i \max(0, \eta - \eta_{u+1})) - \exp(\Gamma_i \max(0, \eta - \eta_u))] \Gamma_i \mathbf{1}\theta_{b,i,u} \quad (45)$$

where $\eta_{i,u} = (D_{i,u} - D_i)/L_i$ is the normalized depth of segment u along borehole i and $\eta_{i,n_{q,i}+1} = 1$.

A relation between the inlet and outlet fluid temperature is obtained by first considering the connection between the pipes at the bottom of the borehole:

$$\Theta_{fd,i}(1) = \Theta_{fu,i}(1) \quad (46)$$

where $\Theta_{fd,i}(\eta) = [\mathbf{I}_{n_{p,i}} \quad \mathbf{0}_{n_{p,i}}] \Theta_{f,i}(\eta)$ is a vector of fluid temperatures in downward flowing pipes, $\Theta_{fu,i}(\eta) = [\mathbf{0}_{n_{p,i}} \quad \mathbf{I}_{n_{p,i}}] \Theta_{f,i}(\eta)$ is a vector of fluid temperatures in upward flowing pipes, $\mathbf{I}_{n_{p,i}}$ is the $n_{p,i} \times n_{p,i}$ identity matrix and $\mathbf{0}_{n_{p,i}}$ is the $n_{p,i} \times n_{p,i}$ null matrix.

The dimensionless fluid temperature vector may be reconstructed by the vectors of fluid temperatures in downward and upward flowing pipes:

$$\Theta_{f,i}(\eta) = [\Theta_{fd,i}^T(\eta) \quad \Theta_{fu,i}^T(\eta)]^T = [\mathbf{I}_{n_{p,i}} \quad \mathbf{0}_{n_{p,i}}]^T \Theta_{fd,i}(\eta) + [\mathbf{0}_{n_{p,i}} \quad \mathbf{I}_{n_{p,i}}]^T \Theta_{fu,i}(\eta) \quad (47)$$

From Equations 45, 46 and 47:

$$\mathbf{E}_{fu,i}^{\theta_u}(1) \Theta_{fu,i}(0) = \mathbf{E}_{fd,i}^{\theta_u}(1) \Theta_{fd,i}(0) + \mathbf{E}_{b,i}^{\theta_u}(1) \bar{\Theta}_{b,i} \quad (48)$$

$$\mathbf{E}_{fu,i}^{\theta_u}(\eta) = [\mathbf{I}_{n_{p,i}} \quad -\mathbf{I}_{n_{p,i}}] \exp(\Gamma_i \eta) [\mathbf{0}_{n_{p,i}} \quad \mathbf{I}_{n_{p,i}}]^T \quad (49)$$

$$\mathbf{E}_{fd,i}^{\theta_u}(\eta) = [-\mathbf{I}_{n_{p,i}} \quad \mathbf{I}_{n_{p,i}}] \exp(\Gamma_i \eta) [\mathbf{I}_{n_{p,i}} \quad \mathbf{0}_{n_{p,i}}]^T \quad (50)$$

$$\mathbf{E}_{b,i}^{\theta_u}(\eta) = [\mathbf{E}_{b,i,1}^{\theta_u}(\eta) \quad \cdots \quad \mathbf{E}_{b,i,n_{q,i}}^{\theta_u}(\eta)] \quad (51)$$

$$\mathbf{E}_{b,i,u}^{\theta_u}(\eta) = [-\mathbf{I}_{n_{p,i}} \quad \mathbf{I}_{n_{p,i}}] \Gamma_i^{-1} [\exp(\Gamma_i \max(0, \eta - \eta_{u+1})) - \exp(\Gamma_i \max(0, \eta - \eta_u))] \Gamma_i \mathbf{1} \quad (52)$$

Expressions for outlet fluid temperatures and fluid temperature profiles based on the inlet fluid temperature are then developed by considering the piping connections within the borehole.

U-tubes in series

For U-tubes connected in series, the inlet of each pipe $m + 1$ ($m \leq n_{p,i} - 1$) is connected to the outlet of pipe $m + n_{p,i}$, $\theta_{f,i,m+n_{p,i}}(0) = \theta_{f,i,m+1}(0)$, the inlet fluid temperature into pipe 1 is equal to the inlet fluid temperature into the borehole, $\theta_{f,i,1}(0) = \theta_{f,in,i}$, and the outlet fluid temperature of pipe $2n_{p,i}$ is equal to the outlet fluid temperature from the borehole, $\theta_{f,i,2n_{p,i}}(0) = \theta_{f,out,i}$. In matrix notation:

$$\Theta_{fd,i}(0) = [1 \quad \mathbf{0}_{1 \times n_{p,i}-1}]^T \theta_{f,in,i} + \mathbf{I}_{n_{p,i}}^{(-1)} \Theta_{fu,i}(0) \quad (53)$$

$$\theta_{f,out,i} = [\mathbf{0}_{1 \times n_{p,i}-1} \quad 1] \Theta_{fu,i}(0) \quad (54)$$

where $\mathbf{I}_{n_{p,i}}^{(-1)}$ is a $n_{p,i} \times n_{p,i}$ matrix with ones along the first diagonal below the main diagonal.

The dimensionless outlet fluid temperature is given by introducing Equations 53 and 54 into Equation 48:

$$\left(\mathbf{E}_{fu,i}^{\theta_u}(1) - \mathbf{E}_{fd,i}^{\theta_u}(1)\mathbf{I}_{n_{p,i}}^{(-1)}\right)\boldsymbol{\Theta}_{fu,i}(0) = \mathbf{E}_{fd,i}^{\theta_u}(1)[1 \quad \mathbf{0}_{1 \times n_{p,i}-1}]^T \theta_{f,\text{in},i} + \mathbf{E}_{b,i}^{\theta_u}(1)\bar{\boldsymbol{\Theta}}_{b,i} \quad (55)$$

$$\theta_{f,\text{out},i} = \mathbf{E}_{\text{in},i}^{\theta_{out}} \theta_{f,\text{in},i} + \mathbf{E}_{b,i}^{\theta_{out}} \bar{\boldsymbol{\Theta}}_{b,i} \quad (56)$$

$$\mathbf{E}_{\text{in},i}^{\theta_{out}} = [\mathbf{0}_{1 \times n_{p,i}-1} \quad 1] \left(\mathbf{E}_{fu,i}^{\theta_u}(1) - \mathbf{E}_{fd,i}^{\theta_u}(1)\mathbf{I}_{n_{p,i}}^{(-1)}\right)^{-1} \mathbf{E}_{fd,i}^{\theta_u}(1)[1 \quad \mathbf{0}_{1 \times n_{p,i}-1}]^T \quad (57)$$

$$\mathbf{E}_{b,i}^{\theta_{out}} = [\mathbf{0}_{1 \times n_{p,i}-1} \quad 1] \left(\mathbf{E}_{fu,i}^{\theta_u}(1) - \mathbf{E}_{fd,i}^{\theta_u}(1)\mathbf{I}_{n_{p,i}}^{(-1)}\right)^{-1} \mathbf{E}_{b,i}^{\theta_u}(1) \quad (58)$$

The fluid temperatures at the top of the boreholes are obtained by introducing Equations 53 and 55 into Equation 47:

$$\boldsymbol{\Theta}_{f,i}(0) = \mathbf{E}_{\text{in},i}^{\theta_0} \theta_{f,\text{in},i} + \mathbf{E}_{b,i}^{\theta_0} \bar{\boldsymbol{\Theta}}_{b,i} \quad (59)$$

$$\mathbf{E}_{\text{in},i}^{\theta_0} = [1 \quad \mathbf{0}_{1 \times n_{p,i}-1}]^T + [\mathbf{I}_{n_{p,i}} \quad \mathbf{I}_{n_{p,i}}^{(-1)}]^T \left(\mathbf{E}_{fu,i}^{\theta_u}(1) - \mathbf{E}_{fd,i}^{\theta_u}(1)\mathbf{I}_{n_{p,i}}^{(-1)}\right)^{-1} \mathbf{E}_{fd,i}^{\theta_u}(1)[1 \quad \mathbf{0}_{1 \times n_{p,i}-1}]^T \quad (60)$$

$$\mathbf{E}_{b,i}^{\theta_0} = [\mathbf{I}_{n_{p,i}} \quad \mathbf{I}_{n_{p,i}}^{(-1)}]^T \left(\mathbf{E}_{fu,i}^{\theta_u}(1) - \mathbf{E}_{fd,i}^{\theta_u}(1)\mathbf{I}_{n_{p,i}}^{(-1)}\right)^{-1} \mathbf{E}_{b,i}^{\theta_u}(1) \quad (61)$$

Fluid temperature profiles are then obtained by introducing Equation 59 into Equation 45:

$$\boldsymbol{\Theta}_{f,i}(\eta) = \mathbf{E}_{\text{in},i}^{\theta}(\eta) \theta_{f,\text{in},i} + \mathbf{E}_{b,i}^{\theta}(\eta) \bar{\boldsymbol{\Theta}}_{b,i} \quad (62)$$

$$\mathbf{E}_{\text{in},i}^{\theta}(\eta) = \exp(\boldsymbol{\Gamma}_i \eta) \mathbf{E}_{\text{in},i}^{\theta_0} \quad (63)$$

$$\mathbf{E}_{b,i}^{\theta}(\eta) = \exp(\boldsymbol{\Gamma}_i \eta) \mathbf{E}_{b,i}^{\theta_0} + [\mathbf{E}_{b,i,1}^{\theta}(\eta) \quad \cdots \quad \mathbf{E}_{b,i,n_{q,i}}^{\theta}(\eta)] \quad (64)$$

$$\mathbf{E}_{b,i,u}^{\theta}(\eta) = \boldsymbol{\Gamma}_i^{-1} [\exp(\boldsymbol{\Gamma}_i \max(0, \eta - \eta_{u+1})) - \exp(\boldsymbol{\Gamma}_i \max(0, \eta - \eta_u))] \boldsymbol{\Gamma}_i \mathbf{1} \quad (65)$$

U-tubes in parallel

For U-tubes connected in parallel, the inlet fluid temperature into each pipe m ($m \leq n_{p,i}$) is equal to the inlet fluid temperature into the borehole, $\theta_{f,i,1}(0) = \theta_{f,\text{in},i}$, and the outlet fluid temperature of the borehole is the result of mixing of the outlets of all pipes m ($m \geq n_{p,i} + 1$). In matrix notation:

$$\boldsymbol{\Theta}_{fd,i}(0) = \mathbf{1} \theta_{f,\text{in},i} \quad (66)$$

$$\theta_{f,out,i} = \frac{Y_i}{\gamma_i} \Theta_{fu,i}(0) \quad (67)$$

where $\mathbf{1}$ is a vector of ones and $\mathbf{Y}_i = [\gamma_{i,1} \quad \cdots \quad \gamma_{i,n_{p,i}}]$ is a vector of dimensionless fluid mass flow rates in each U-tube, with $\gamma_{i,m} = \dot{m}_{i,m} c_p / 2\pi k_s L_i$.

The dimensionless outlet fluid temperature is given by introducing Equations 66 and 67 into Equation 48:

$$\Theta_{fu,i}(0) = \mathbf{E}_{fu,i}^{\theta_u -1}(1) \mathbf{E}_{fd,i}^{\theta_u}(1) \mathbf{1} \theta_{f,in,i} + \mathbf{E}_{fu,i}^{\theta_u -1}(1) \mathbf{E}_{b,i}^{\theta_u}(1) \bar{\Theta}_{b,i} \quad (68)$$

$$\theta_{f,out,i} = \mathbf{E}_{in,i}^{\theta_{out}} \theta_{f,in,i} + \mathbf{E}_{b,i}^{\theta_{out}} \bar{\Theta}_{b,i} \quad (69)$$

$$\mathbf{E}_{in,i}^{\theta_{out}} = \frac{Y_i}{\gamma_i} \mathbf{E}_{fu,i}^{\theta_u -1}(1) \mathbf{E}_{fd,i}^{\theta_u}(1) \mathbf{1} \quad (70)$$

$$\mathbf{E}_{b,i}^{\theta_{out}} = \frac{Y_i}{\gamma_i} \mathbf{E}_{fu,i}^{\theta_u -1} \mathbf{E}_{b,i}^{\theta_u}(1) \quad (71)$$

The fluid temperatures at the top of the boreholes are obtained by introducing Equations 66 and 68 into Equation 47:

$$\Theta_{f,i}(0) = \mathbf{E}_{in,i}^{\theta_0} \theta_{f,in,i} + \mathbf{E}_{b,i}^{\theta_0} \bar{\Theta}_{b,i} \quad (72)$$

$$\mathbf{E}_{in,i}^{\theta_0} = [\mathbf{I}_{n_{p,i}} \quad \mathbf{0}_{n_{p,i}}]^T \mathbf{1} + [\mathbf{0}_{n_{p,i}} \quad \mathbf{I}_{n_{p,i}}]^T \mathbf{E}_{fu,i}^{\theta_u -1}(1) \mathbf{E}_{fd,i}^{\theta_u}(1) \mathbf{1} \quad (73)$$

$$\mathbf{E}_{b,i}^{\theta_0} = [\mathbf{0}_{n_{p,i}} \quad \mathbf{I}_{n_{p,i}}]^T \mathbf{E}_{fu,i}^{\theta_u -1}(1) \mathbf{E}_{b,i}^{\theta_u}(1) \quad (74)$$

Appendix 2 : Coefficients for the evaluation of heat extraction rates

The average heat extraction rate per unit borehole length of a segment u of a borehole i is obtained from an energy balance on the fluid flowing in each of the pipes:

$$\bar{\phi}'_{i,u} = [\mathbf{Y}_i \quad -\mathbf{Y}_i] \left(\Theta_{f,i}(\eta_{i,u}) - \Theta_{f,i}(\eta_{i,u-1}) \right) \quad (75)$$

where $\eta_{i,u} = (D_{i,u} - D_i)/L_i$ is the normalized depth of segment u along borehole i .

Introducing Equation 62 into Equation 75:

$$\bar{\phi}'_{i,u} = [\mathbf{Y}_i \quad -\mathbf{Y}_i] \left(\mathbf{E}_{\text{in},i}^\theta(\eta_{i,u}) - \mathbf{E}_{\text{in},i}^\theta(\eta_{i,u-1}) \right) \theta_{f,\text{in},i} + [\mathbf{Y}_i \quad -\mathbf{Y}_i] \left(\mathbf{E}_{b,i}^\theta(\eta_{i,u}) - \mathbf{E}_{b,i}^\theta(\eta_{i,u-1}) \right) \bar{\boldsymbol{\Theta}}_{b,i} \quad (76)$$

The heat extraction rates per unit borehole length of all segments of borehole i are then given by assembling Equation 76 for all segments of the borehole:

$$\bar{\boldsymbol{\Phi}}'_i = \mathbf{E}_{\text{in},i}^\phi \theta_{f,\text{in},i} + \mathbf{E}_{b,i}^\phi \bar{\boldsymbol{\Theta}}_{b,i} \quad (77)$$

$$\mathbf{E}_{\text{in},i}^\phi = \begin{bmatrix} \mathbf{E}_{\text{in},i,1}^\phi & \cdots & \mathbf{E}_{\text{in},i,n_{q,i}}^\phi \end{bmatrix}^T \quad (78)$$

$$\mathbf{E}_{\text{in},i,u}^\phi = [\mathbf{Y}_i \quad -\mathbf{Y}_i] \left(\mathbf{E}_{\text{in},i}^\theta(\eta_{i,u}) - \mathbf{E}_{\text{in},i}^\theta(\eta_{i,u-1}) \right) \quad (79)$$

$$\mathbf{E}_{b,i}^\phi = \begin{bmatrix} \mathbf{E}_{b,i,1}^\phi & \cdots & \mathbf{E}_{b,i,n_{q,i}}^\phi \end{bmatrix}^T \quad (80)$$

$$\mathbf{E}_{b,i,u}^\phi = [\mathbf{Y}_i \quad -\mathbf{Y}_i] \left(\mathbf{E}_{b,i}^\theta(\eta_{i,u}) - \mathbf{E}_{b,i}^\theta(\eta_{i,u-1}) \right) \quad (81)$$

Appendix 3 : Sample calculation of the g -function of a field of 2 boreholes

The evaluation of the g -function is carried out by the following process: (1) Identification of borehole and bore field parameters, (2) evaluation of the segment-to-segment thermal response matrix, (3) evaluation of coefficients for fluid temperatures and heat extraction rates in the boreholes, (4) evaluation of coefficients for fluid temperatures and heat extraction rates in the bore field, (5) evaluation of the dimensionless fluid and borehole wall temperatures, (6) evaluation of the effective bore field thermal resistance, and (7) evaluation of the effective dimensionless borehole wall temperature (i.e. the g -function). This appendix outlines this process for the evaluation of the g -function of a field of 2 series-connected boreholes.

Borehole and bore field parameters

The positions and dimensions of boreholes in a field of 2 series-connected boreholes are illustrated on Figure 10. Parameters relevant to the evaluation of the g -function are presented in Table 2. For the purpose of the sample calculation, the g -function is calculated using only $n_{q,1} = n_{q,2} = 1$ segment per borehole and at only two time steps $t_1 = 10000$ h and $t_2 = 20000$ h. The bore field connectivity vector and path sequences are obtained from the bore field layout presented in Figure 10:

$$\mathbf{C}_{in} = [0 \quad 1] \quad (82)$$

$$\mathbf{P}_{in,1} = \{1\}, \mathbf{P}_{in,2} = \{2, 1\} \quad (83)$$

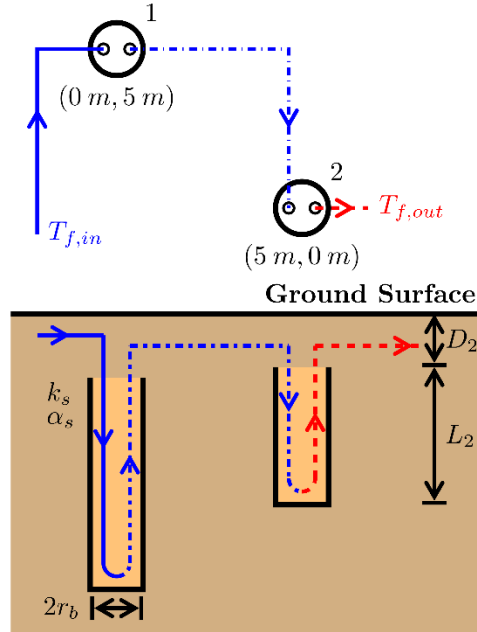


Figure 10. Field of 2 series-connected geothermal boreholes

Table 2. Parameters of the field of 2 boreholes		
Parameter	Value	Units
Bore field		
Number of boreholes, N_b	2	-
Total fluid mass flow rate, \dot{m}	0.25	kg/s
Boreholes		
Borehole lengths, L_1 / L_2	150 / 100	m
Borehole radius, r_b	0.075	m
Borehole buried depths, D_1 / D_2	3 / 2	m
Piping		
Number of U-tubes per borehole, n_n	1	-
Pipe outer diameter	0.0422	m
Pipe inner diameter	0.0294	m
Shank spacing	0.052	m
Pipe surface roughness	10^{-6}	m
Physical properties		
Ground thermal conductivity, k_s	2	W/m-K
Ground thermal diffusivity, α_s	10^{-6}	m ² /s
Grout thermal conductivity	1	W/m-K
Pipe thermal conductivity	0.4	W/m-K
Fluid thermal conductivity	0.492	W/m-K
Fluid density	1015	kg/m ³
Fluid specific heat capacity, c_f	3977	J/kg-K
Fluid dynamic viscosity	0.00203	kg/m-s

Segment-to-segment thermal response matrix

The segment-to-segment thermal response matrices, \mathbf{H} , are obtained from the evaluation of the finite line source solution (Equation 5) for each pair of borehole segments in the bore field and at each time step. The segment-to-segment thermal response factors, $h_{i,j,u,v}$, are then assembled according to Equation 11:

$$\mathbf{H}(t_1) = \begin{bmatrix} 4.7392 & 0.2568 \\ 0.3852 & 4.7119 \end{bmatrix} \quad (84)$$

$$\mathbf{H}(t_2) = \begin{bmatrix} 5.0630 & 0.4250 \\ 0.6374 & 5.0222 \end{bmatrix} \quad (85)$$

Coefficients for fluid temperatures and heat extraction rates in the boreholes

The multipole solution of order 3 is used to evaluate delta-circuit thermal resistances (Claesson and Hellström 2011) :

$$R_{1,1,1}^{\Delta} = R_{1,2,2}^{\Delta} = R_{2,1,1}^{\Delta} = R_{2,2,2}^{\Delta} = 0.2908 \text{ m-K/W} \quad (86)$$

$$R_{1,1,2}^{\Delta} = R_{1,2,1}^{\Delta} = R_{2,1,2}^{\Delta} = R_{2,2,1}^{\Delta} = -3.2774 \text{ m-K/W} \quad (87)$$

Following the evaluation of the dimensionless delta-circuit thermal resistances, $\Omega_{i,m,n}^{\Delta} = 2\pi k_s R_{i,m,n}^{\Delta}$, and the dimensionless fluid mass flow rates, $\gamma_i = \dot{m}_i c_f / 2\pi k_s L_i$, the dimensionless thermal conductance matrices are evaluated from Equation 20 :

$$\mathbf{\Gamma}_1 = \begin{bmatrix} -0.4728 & -0.0460 \\ 0.0460 & 0.4728 \end{bmatrix} \quad (88)$$

$$\mathbf{\Gamma}_2 = \begin{bmatrix} -0.3152 & -0.0307 \\ 0.0307 & 0.3152 \end{bmatrix} \quad (89)$$

As the two boreholes are single U-tube boreholes, the coefficients for the evaluation of the dimensionless outlet fluid temperatures of the boreholes (Equation 22) can be obtained by either of Equations 57 and 58, or Equations 70 and 71 :

$$E_{in,1}^{\theta_{out}} = 0.3481 \quad (90)$$

$$\mathbf{E}_{b,1}^{\theta_{out}} = [0.6519] \quad (91)$$

$$E_{in,2}^{\theta_{out}} = 0.4981 \quad (92)$$

$$E_{b,2}^{\theta_{out}} = [0.5018] \quad (93)$$

The coefficients for the evaluation of the normalized heat extraction rates of the boreholes (Equation 23) are obtained from Equation 78 and 80 :

$$E_{in,1}^{\phi} = [0.3439] \quad (94)$$

$$E_{b,1}^{\phi} = [-0.3439] \quad (95)$$

$$E_{in,2}^{\phi} = [0.3970] \quad (96)$$

$$E_{b,2}^{\phi} = [-0.3970] \quad (97)$$

Coefficients for fluid temperatures and heat extraction rates in the bore field

The coefficients for the evaluation of the normalized heat extraction rates of the bore field (Equation 29) are obtained from Equation 27 and assembled according to Equations 30 and 31 :

$$A_{in}^{\phi} = [0.3439 \quad 0.1382]^T \quad (98)$$

$$A_b^{\phi} = \begin{bmatrix} -0.3439 & 0 \\ 0.2588 & -0.3970 \end{bmatrix} \quad (99)$$

The coefficients for the evaluation of the dimensionless outlet fluid temperature of the bore field (Equation 34) are then obtained from Equation 33 :

$$A_{in}^{\theta_{out}} = 0.1734 \quad (100)$$

$$A_b^{\theta_{out}} = [0.3248 \quad 0.5018] \quad (101)$$

Dimensionless fluid and borehole wall temperatures

The system of equations of Equation 36 is assembled and solved sequentially for each time step. Note that the zero-extraction dimensionless borehole wall temperatures, $\bar{\Theta}_{b,k}^0$, change every time step. The

segment-to-segment thermal response matrix, \mathbf{H} , only changes if the time step changes. At the first time step

$t = t_1$:

$$\begin{bmatrix} 4.7392 & 0.2568 & -1 & 0 & 0 \\ 0.3852 & 4.7119 & 0 & -1 & 0 \\ -1 & 0 & -0.3439 & 0 & 0.3439 \\ 0 & -1 & 0.2588 & -0.3970 & 0.1382 \\ 0.6 & 0.4 & 0 & 0 & 0 \end{bmatrix} \begin{bmatrix} \bar{\Phi}'_{1,1,1} \\ \bar{\Phi}'_{2,1,1} \\ \bar{\theta}_{b,1,1,1} \\ \bar{\theta}_{b,2,1,1} \\ \theta_{f,in,1} \end{bmatrix} = \begin{bmatrix} 0 \\ 0 \\ 0 \\ 0 \\ 1 \end{bmatrix} \quad (102)$$

The solution of the system of equations gives normalized heat extractions rates, dimensionless borehole wall temperatures and inlet fluid temperature at time t_1 :

$$\bar{\Phi}'_1 = [1.1016 \quad 0.8476]^T \quad (103)$$

$$\bar{\Theta}_{b,1} = [5.4383 \quad 4.4183]^T \quad (104)$$

$$\theta_{f,in,1} = 8.6416 \quad (105)$$

Starting from the second time step $t = t_2$, the zero-extraction dimensionless borehole wall temperatures are evaluated from Equation 13 (with $t_0 = 0$) :

$$\bar{\Theta}_{b,2}^0 = (\mathbf{H}(t_2 - t_0) - \mathbf{H}(t_2 - t_1))\bar{\Phi}'_1 = [0.4993 \quad 0.5409]^T \quad (106)$$

The solution of the updated system of equations gives normalized heat extractions rates, dimensionless borehole wall temperatures and inlet fluid temperature at time t_2 :

$$\bar{\Phi}'_2 = [1.1042 \quad 0.8437]^T \quad (107)$$

$$\bar{\Theta}_{b,2} = [5.9490 \quad 4.9416]^T \quad (108)$$

$$\theta_{f,in,2} = 9.1600 \quad (109)$$

Effective dimensionless bore field thermal resistances

The effective dimensionless bore field thermal resistance is evaluated from Equation 40 :

$$\Omega_{field}^* = 2.2427 \quad (110)$$

Effective dimensionless borehole wall temperature

The effective dimensionless borehole wall temperature is finally evaluated from Equation 41 :

$$\theta_b^*(t_1) = 4.8191 \quad (111)$$

$$\theta_b^*(t_2) = 5.3374 \quad (112)$$

List of figure captions

Figure 1. Field of 3 vertical geothermal boreholes

Figure 2. Delta-circuit of thermal resistances of a double U-tube borehole

Figure 3. Bore field of 144 boreholes in 24 parallel branches of 6 series-connected boreholes

Figure 4. Comparison of the dimensionless effective borehole wall and inlet fluid temperatures with the DST model

Figure 5. Inlet fluid temperature during the 5th simulation year (above), and average heat extraction rate per unit borehole length (below)

Figure 6. Comparison of the inlet fluid temperatures predicted by the g-function and the DST model (above), difference between the two models (center), and average heat extraction rate per unit borehole length (below)

Figure 7. Influence of the dimensionless fluid mass flow rate on the dimensionless inlet fluid temperature and on the effective dimensionless borehole wall temperature

Figure 8. Influence of the dimensionless fluid mass flow rate on the steady-state dimensionless effective borehole wall temperature and on the steady-state dimensionless inlet fluid temperature

Figure 9. Influence of the dimensionless fluid mass flow rate on the effective borehole thermal resistance and the effective bore field thermal resistance

Figure 10. Field of 2 series-connected geothermal boreholes

List of table titles

Table 1. Parameters of the bore field

Table 2. Parameters of the field of 2 boreholes